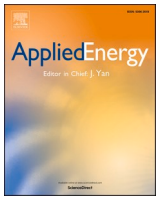
Applied Energy 427 (2027) 129200



Contents lists available at ScienceDirect

Applied Energy

journal homepage: www.elsevier.com/locate/apenergy



Advances in sorption-based thermochemical energy storage: from material properties to prototype-level performance

Mingxi Ji [a], Zhixiong Ding [b,*], Jinhan Mo [c,d,e], Yulong Ding [a]

[a] Birmingham Centre for Energy Storage & School of Chemical Engineering, University of Birmingham, Birmingham B15 2TT, UK
[b] State Key Laboratory of Intelligent Geotechnics and Tunnelling, College of Civil and Transportation Engineering, Shenzhen University, Shenzhen, Guangdong 518060, China
[c] Key Laboratory of Coastal Urban Resilient Infrastructures (Ministry of Education), College of Civil and Transportation Engineering, Shenzhen University, Shenzhen, Guangdong 518060, China
[d] State Key Laboratory of Subtropical Building and Urban Science, Shenzhen University, Shenzhen, Guangdong 518060, China
[e] Key Laboratory of Coastal Urban Soil-Water Environmental Evolution, Ministry of Ecology and Environment (under construction), Shenzhen University, Shenzhen, Guangdong 518060, China

HIGHLIGHTS

- Systematically bridges material properties with S-TCES system performance.
- Quantifies a 52–56% energy density reduction from material to prototype scale.
- Characterization and performance evaluation of adsorbent materials are reviewed.
- The innovations of state-of-the-art open and closed reactors are reviewed.
- Proposes lab-scale dynamic prototyping to replace static characterization.

ARTICLE INFO

Keywords:
Thermochemical energy storage
sorption
adsorbent
material-level
prototype-level

ABSTRACT

This review focuses on solid-gas sorption-based thermochemical energy storage (S-TCES). S-TCES has gained increasing attention in recent decades as a promising thermal energy storage and heat decarbonisation solution, particularly for high-energy-density long-duration energy storage applications, which are crucial for waste heat utilisation and future renewable-dominated energy systems. However, a notable gap exists between the theoretical performance of adsorbents, as measured at the material level and the actual performance in practical S-TCES systems. This gap has hindered practical material selection, the design of practical systems, and the prediction of performance at the prototype level. This article offers a systematic and critical analysis of recent advancements in S-TCES, bridging material properties with prototype-level performance. A framework is established, encompassing adsorbent classification, key selection criteria, and fundamental characterisation methods. A comparative analysis is conducted on representative physical, chemical, and composite adsorbents with respect to their thermodynamic properties, sorption behaviour, and transport characteristics. Furthermore, the operational performance of the state-of-the-art open and closed S-TCES prototypes is analysed. A cross-literature statistical comparison reveals that the volumetric ESD of the surveyed prototypes is approximately 52–56% lower than that of the material-level dataset, quantitatively highlighting the substantial gap between material characterization and prototype performance. This work clarifies the relationship between fundamental material properties and practical system performance, offering valuable insights for material scientists and system engineers.

1. Introduction

The escalating energy crisis and environmental degradation have

* Corresponding author.
E-mail address: zhixding@szu.edu.cn (Z. Ding).

https://doi.org/10.1016/j.apenergy.2026.129200
Received 24 August 2026; Received in revised form 14 October 2026; Accepted 26 October 2026
0306-2619/© 2026 Elsevier Ltd. All rights are reserved, including those for text and data mining, AI training, and similar technologies.

Nomenclature

Variables

t_a	adsorption temperature, °C
t_c	condensation temperature, °C
t_e	evaporation temperature, °C
t_g	generation temperature, °C

Abbreviations

COF	covalent organic framework
DVS	dynamic vapor sorption
ESD	energy storage density
EVM	expanded vermiculite
MIL	materials of Institute Lavoisier framework, a zirconium-based MOF
MOF	metal-organic framework
RH	relative humidity
STA	simultaneous thermal analyzer
TCES	thermochemical energy storage
TEM	transmission electron microscopy
XRD	X-ray diffraction
DSC	differential scanning calorimetry
ENG-TSA	expanded natural graphite treated with sulfuric acid
ESE	energy storage efficiency
HTF	heat transfer fluid
MIP	molecularly imprinted polymer
PCM	phase change material
SEM	scanning electron microscopy
S-TCES	sorption-based thermochemical energy storage
TES	thermal energy storage
TG	thermogravimetric analysis

become persistent global challenges [1]. Consequently, increasing the utilization of renewable energy and waste heat is not only an imperative step toward achieving carbon neutrality [2] but also the key to resolving these dual dilemmas [3,4]. However, the inherent timing and intensity mismatch between renewable/waste energy sources and demand prevents direct utilization of these resources [5]. To bridge this gap, energy storage technologies are essential for integrating and regulating these fluctuating renewable/waste energy flows [6].

1.1. Classification of thermal energy storage technologies

Because heating and cooling demand over half of terminal energy

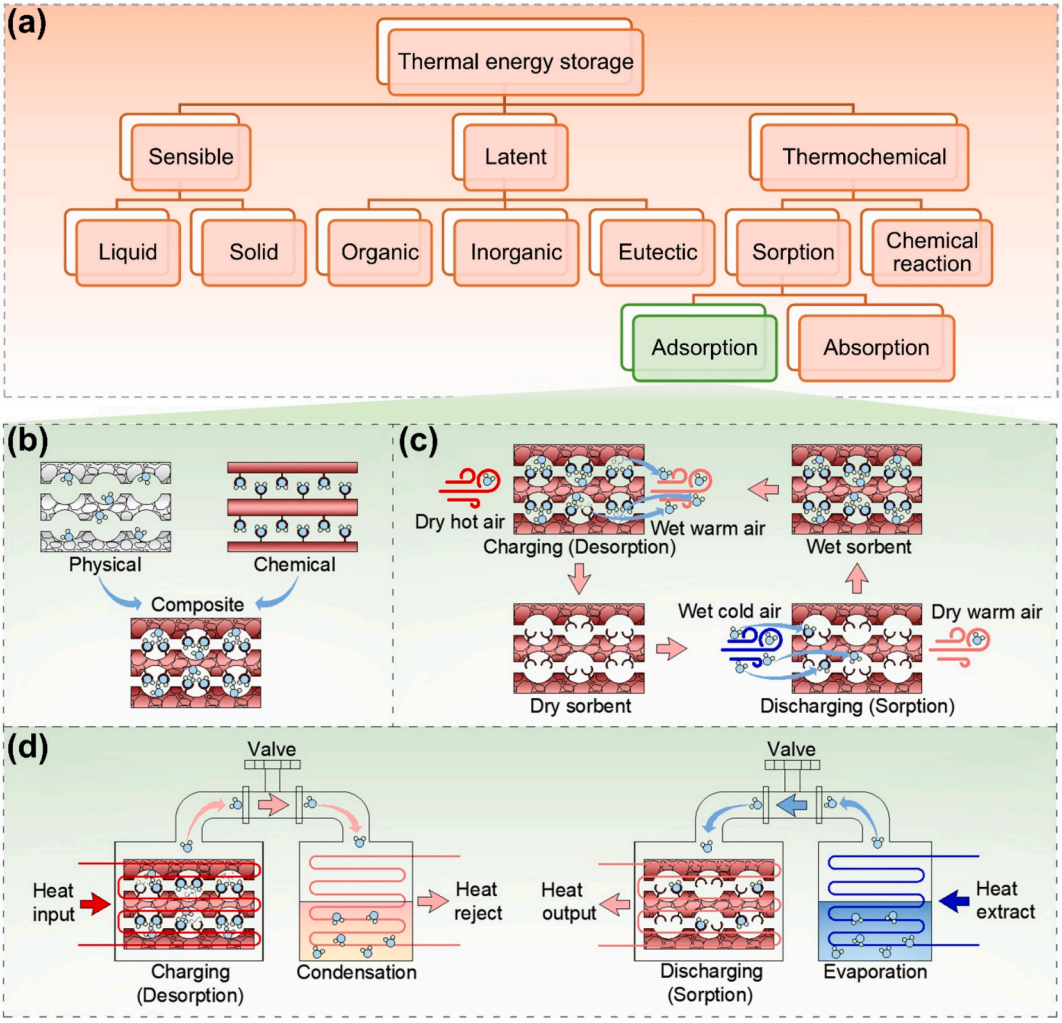


Fig. 1. TES technologies and sorption mechanisms: (a) classification of current TES technologies, (b) physical, chemical and composite sorption mechanisms, (c) working principle of open S-TCES, (d) working principle of closed S-TCES.

consumption [7], thermal energy storage (TES) technologies tailored to end-use requirements have garnered widespread attention in recent years [8]. Based on the underlying operating principles, TES technologies are generally classified as sensible TES, latent TES, and thermochemical TES [9,10] (as illustrated in Fig. 1(a)).

Sensible TES stores thermal energy via temperature changes in liquid (e.g., water, oil) or solid (e.g., rock, cement, molten salts) materials [11]. While sensible TES is characterized by simple principles, technological maturity, and low cost [12], leading to its extensive application in practical projects, its low energy storage density (ESD) and significant heat losses render it increasingly ill-suited for dense urban environments where space is a constraint [13]. Latent TES utilizes the endothermic and exothermic processes associated with phase transitions to store heat, most commonly solid-liquid transitions. Phase change materials (PCMs) mainly include organic (e.g., paraffin, fatty acids), inorganic (e.g., hydrated salts, water), and organic-inorganic deep eutectic solvents [14]. Due to the high latent heat of phase change, latent TES offers a significantly higher ESD than sensible TES while maintaining a relatively simple system structure [15]. Consequently, latent TES has been a focal point in the TES research community over the past decades [14], with studies ranging from the development of novel PCMs and the modification of existing PCMs to the optimization of heat exchangers and potential application systems [16]. Nevertheless, the large-scale application of latent TES remains restricted by intrinsic material limitations: the low thermal conductivity of organic materials results in slow charging/discharging rates [17]; the high degree of supercooling in inorganic materials causes delayed energy release [18], affecting system responsiveness and efficiency; and deep eutectic solvents often suffer from poor thermal stability [19].

Thermochemical TES is widely regarded as the future of thermal energy storage due to its high ESD [20]; however, there are currently few practical applications due to its low technology readiness level [21]. Thermochemical TES can be further categorized into chemical reaction TES and sorption-based TES, also known as sorption-based thermochemical energy storage (S-TCES) [22]. Many chemical-reaction TES systems operate at relatively high temperatures, although the required charging temperature strongly depends on the specific reversible reaction pair, resulting in a poor match with common low-grade renewable sources (e.g., solar energy) and waste heat [23]. In contrast, sorption-based TES, which is based on liquid absorption and solid adsorption, shows advantages in low charging temperatures (typically below 150°C, even as low as 50°C [24]) and possesses ESD significantly higher than both sensible and latent TES [25]. Furthermore, because thermal energy is stored as sorption potential, heat losses during even seasonal storage are negligible [26]. Sorption-based TES also offers superior output flexibility with heat input, capable of providing heating, cooling, or dehumidification [27]. While liquid absorption-based and solid adsorption-based TES share similar principles, the main distinction lies in the sorption materials, which dictate subsequent components and system design. Compared to liquid absorption-based TES, solid adsorption-based TES eliminates the need for liquid spraying systems [28]. This results in a more compact device structure with fewer moving parts (e.g., pumps), thereby reducing the noise and the probability of failure. Note that adsorption-based TES is the focus of this work and is referred to as S-TCES.

1.2. Working principle of S-TCES

The fundamental operation of S-TCES relies on the reversible interaction between an adsorbate (typically water vapor or ammonia) and a solid adsorbent [29]. Based on underlying microscopic mechanisms, sorption is classified as physical or chemical [30]. Physical adsorbents, such as silica gel, zeolites, metal-organic frameworks (MOFs), and covalent organic frameworks (COFs), capture moisture within their porous structures via weak van der Waals forces [31]. In contrast, chemical adsorbents rely on forming and breaking chemical bonds to store energy, typically offering higher ESD but often suffering from stability issues such as swelling or agglomeration. To synergize the advantages of both mechanisms and enhance the sorption capacity per unit volume, composite adsorbents have been developed. As illustrated in Fig. 1(b), these materials are synthesized by impregnating porous physical matrices with chemical salts, thereby increasing ESD while potentially improving mass transfer relative to bulk salts by dispersing the active salt within an accessible porous network. However, compared with the pristine porous host, excessive salt loading may block pore channels and increase mass-transfer resistance [32].

S-TCES systems are generally classified into two configurations: open and closed systems. The open system, characterized by the direct contact between the adsorbent and the airflow, operates under atmospheric pressure and is structurally simpler. Fig. 1(c) schematically illustrates the operational cycle of an open S-TCES system, which consists of a charging (desorption) phase and a discharging (adsorption) phase [33,34]. Here, an example of an adsorbent and water working pair was used in the demonstration of the mechanism. During charging, an external heat source generates a stream of dry, hot air that is blown through the adsorbent bed. This allows thermal energy to drive the water molecules out of the porous structure, carrying the moisture away into the environment. Consequently, the sorption potential of the adsorbent material is regenerated, and the input thermal energy is effectively stored as sorption capacity within the dried adsorbent bed. Conversely, during discharge, wet, cold air is directed through the dry adsorbent bed. The adsorbent material captures moisture from the airstream due to its high affinity for water vapor. This sorption process is exothermic, thus releasing the stored heat and significantly raising the air temperature. The resulting output is a stream of dry, warm air that can be utilized directly for space heating applications [35].

In contrast to the open configuration, the closed S-TCES system operates in isolation from the atmosphere. As depicted in Fig. 1(d), the system is hermetically sealed and evacuated to remove non-condensable gases [36]. It primarily consists of two connected hermetically sealed vessels: one packed with the adsorbent (referred to as the reactor) and the other serving to store the adsorbate (commonly water, which acts as the refrigerant). During charging, the system regenerates the adsorbent. An external heat source supplies thermal energy to the adsorbent bed indirectly via internal heat exchangers (e.g., coils or finned tubes). The temperature increase triggers the desorption of water vapor from the adsorbent. Driven by the pressure difference, the vapor flows through the connecting pipe into the refrigerant vessel (acting as a condenser), where it is condensed by a cooling water loop and stored in liquid form. Similar to the open system, this process increases the dryness of the adsorbent, thereby increasing its sorption potential to store thermal energy. During discharge, the regenerated (dry) adsorbent has a strong affinity for water molecules, maintaining a low vapor pressure within the closed system. This low-pressure environment facilitates continuous evaporation of the liquid refrigerant, extracting low-grade heat from the ambient environment or a low-temperature waste heat source. The vapor is then adsorbed by the bed, releasing the sorption heat, which is recovered via the heat exchanger for heating applications. Notably, the closed system offers versatile functionality: in addition to heating, the cooling effect produced during refrigerant evaporation can be used for refrigeration or air conditioning [37]. Table 1 summarizes the fundamental distinctions between the two system configurations in terms of operation, structure, and application potential.

1.3. Development status of S-TCES

To bridge the gap between theoretical potential and practical application, research efforts to advance S-TCES technology have primarily focused on three developmental pathways: adsorbent material development, sorption bed optimization, and thermodynamic cycle innovation [30,39], as shown in Fig. 2.

S-TCES technologies still lack widespread, large-scale applications,

Table 1
Comparison of open and closed S-TCES systems [30,38].

Feature	Open S-TCES system	Closed S-TCES system
Operating environment	Atmospheric pressure	Hermetically sealed to exclude non-condensable gases
Working fluid (adsorbate)	Moisture in the air	Pure refrigerant vapor (e.g., water, ammonia)
Heat transfer fluid	Air flows directly through the adsorbent bed	Water or oil flows through heat exchangers (e.g., coil, finned tubes)
System complexity	Simple structure, no need for vacuum pumps or complex sealing	Requires hermetic, pressure-compatible vessels, internal heat exchangers, and possibly pumps for refrigerant circulation
Energy output	Dry and warm air: space heating and dehumidification	Capable of space heating, cooling, and domestic hot water
Integration flexibility	Limited by ambient humidity levels; performance fluctuates with weather conditions	Independent of ambient humidity; performance is more stable and controllable

primarily because of the intrinsic limitations of current adsorbents. These limitations include poor heat and mass transfer performance, high regeneration temperature requirements, low hydrothermal stability, and prohibitive costs [46]. Furthermore, long-term stability remains a critical issue; during repeated adsorption-desorption cycles, adsorbents often suffer from performance attenuation. A common failure mode is physical agglomeration, where originally loose particles clump into solid blocks after multiple cycles, leading to increased pressure drop and drastic efficiency degradation [47]. Therefore, advancing materials research to develop robust, high-performance adsorbents remains the pivotal pathway to overcome these bottlenecks and realize large-scale commercialization of S-TCES. A major progress occurred with the development of composite sorbents. Impregnating hygroscopic salts into porous matrix host materials (such as expanded graphite, silica gel, and carbon nanotubes) significantly enhanced heat/mass transfer and mitigated structural coalescence. With their ultra-high specific surface area, highly tunable pore structures, and lower operating temperatures, MOFs have recently emerged as leading candidates for sorption-based thermal storage. Recent advances primarily focus on tailoring host-guest interactions via molecular engineering and machine-learning-guided screening, substantially enhancing both hydrothermal stability and sorption kinetics under mild regeneration conditions.

The second pathway focuses on sorption bed optimization, which is essential for translating theoretical material potential into effective prototype-level operation. While small-scale samples typically exhibit peak adsorption and desorption kinetics, the scale-up to full S-TCES systems introduces significant challenges. In bulk-packed beds, the dense accumulation of adsorbents creates inter-particle interference and resistance, leading to a substantial attenuation in heat and mass transfer. To mitigate these negative effects, structural optimizations are employed to enhance transport processes. Typical strategies include the use of multi-layer bed configurations [48,49], which reduce bed thickness and maximize the contact surface area to facilitate airflow and diffusion. For systems utilizing internal heat exchangers, the most prevalent approach involves equipping the piping with fins to augment the heat transfer surface area and thermal conductivity [50].

The third pathway involves the design of advanced thermodynamic cycles to tailor system performance to specific boundary conditions. For instance, the double-stage cycle has been introduced to boost the output temperature, enhancing the system's resilience against low ambient temperatures and enabling effective heating in cold climates [51]. Similarly, the compression-assisted cycle incorporates compressors to strengthen desorption or adsorption. This mechanical enhancement

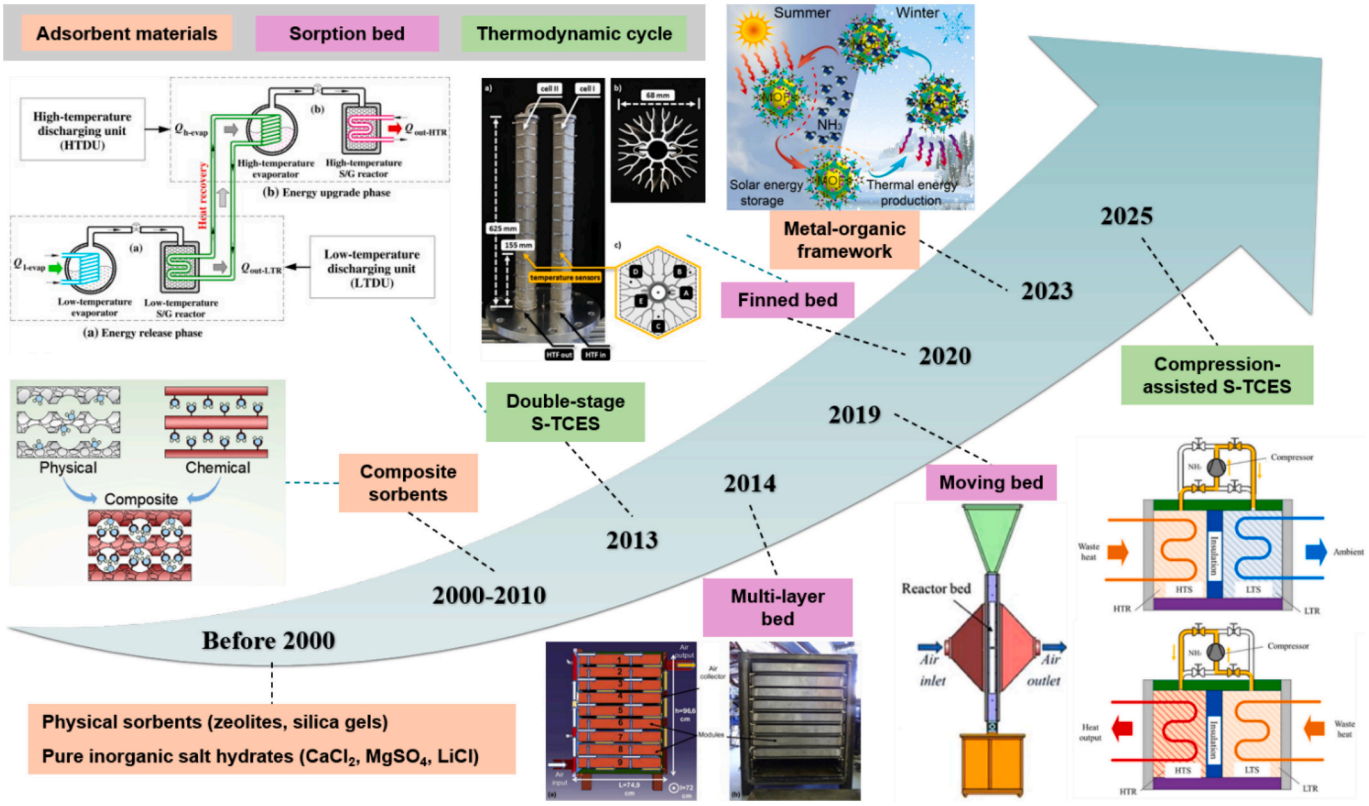


Fig. 2. The development roadmap of S-TCES technologies. Adapted with permission from Ref. [40], Copyright 2013 Elsevier; adapted with permission from Ref. [41], Copyright 2014 Elsevier; adapted with permission from Ref. [42], Copyright 2019 Elsevier; adapted with permission from Ref. [43], Copyright 2020 Elsevier; adapted with permission from Ref. [44], Copyright 2023 Elsevier; adapted with permission from Ref. [45], Copyright 2025 Elsevier.

Table 2
Summary and comparison of representative studies addressing material- and prototype-level performance in S-TCES.

Ref.	Primary scope		Main contents covered	Key findings	Material-to-prototype gap quantified?
	material	prototype			
[54]	√	×	Review of adsorbents, evaluation of stability, safety, and material costs	Highlighted $MgSO_4$ and binary salt composites as high-capacity options.	× Material/Salt-hydrate focus
[55]	√	×	Review of water-based adsorbents for low-temperature space heating	Categorized adsorbents for moist-air open systems; suggested adsorption suitability primarily for seasonal auxiliary heating.	× Application-specific material focus
[56]	×	√	Review of systems and performance, evaluation via temperature effectiveness	The closed-transported system exhibits better performance; demonstrated the inadequacy of volumetric ESD for cross-system comparisons.	× Process metric focus
[57]	×	√	Review of multistage and cascaded S-TCES cycles and prototypes	Demonstrated superior performance of cascaded systems for solar/waste heat; identified high costs and scarce physical prototypes as key barriers.	× Cycle multi-staging focus
[58]	√	√	Review of advanced adsorbents and demonstrative projects	Identified top-performing impregnated sorbents; highlighted economic unviability and material degradation as major barriers.	× Material and project overview
[59]	√	√	Review of sorbents, open/closed cycle architectures, reactor/heat exchanger design strategies, prototype operation performance	Identified severe output temperature instability and key prototype-level volume penalties; highlighted heat/mass transfer degradation.	× Qualitative scale-gap discussion
[60]	√	√	Review of ammonia sorbents (metal salts, composites), prototype development and specialized application scenarios	Highlighted ammonia's versatility for sub-zero cooling and power generation; detailed trade-offs of metal salts; proposed hybrid cycles to widen operational range.	× Ammonia-focused qualitative review
[61]	√	√	Review of water-based sorbent materials and advanced cycles under application-oriented criteria	Provided application-oriented selection principles of diversified materials and system cycles; outlined the challenges and future outlook	× Application and economic focus
[62]	√	√	Review of sorbent materials, open/closed systems, fixed/moving beds, application scenarios	Emphasized that future progress requires synergistic cross-level design rather than isolated domain advances; proposed AI/digital twins and additive manufacturing to solve cyclic decay and scaling bottlenecks.	× Applications and challenges focus
[63]	√	√	Review of water-based sorption materials and open/closed prototypes	Compared material and prototype performance and identified heat/mass transfer and practical scale-up limitations	× Qualitative scale-gap discussion
[22]	√	√	Methodology for evaluating ESD at material and prototype levels across TES technologies	Demonstrated the influence of component volume and system complexity on ESD using three TES prototypes	√ Not S-TCES-specific literature analysis
This work	√	√	Review of sorbent materials, open/closed prototypes with various sorption beds	Quantified that prototype-realized ESD is on average 54.3% lower than theoretical material-level potential.	√ Material-to-prototype gap quantified

reduces charging temperatures, raises heating temperatures, improves ESD, and allows adjustable output [52,53]. However, while these advanced cycles yield specific performance enhancements, they invariably incur trade-offs. The implementation of a double-stage or compression-assisted system increases structural complexity, operational control difficulty, and overall capital costs [45].

1.4. Novelties and contributions

This article provides a systematic and critical analysis of recent advances in solid adsorption-based thermochemical energy storage, covering adsorbent materials, reactor prototypes, and the transition from material-level properties to prototype-level performance. Table 2 systematically compares representative review articles in the field of S-TCES with this work across their primary scope (material vs. system), main contents covered, key findings, and whether the material-to-prototype performance gap is quantitatively evaluated. While numerous review papers have individually summarized material synthesis or reactor/system configurations for S-TCES, a critical knowledge gap persists in quantitatively bridging the discrepancy between intrinsic material potential and realized prototype performance. Existing literature often conflates ideal lab-scale metrics (e.g., thermodynamic equilibrium capacity) with practical energy storage performance (e.g., volumetric ESD and actual efficiency under mass-transfer constraints), leading to unrealistic expectations and misleading benchmarks.

To address this challenge, this review uniquely focuses on elucidating and quantifying the performance evolution chain from material characterization to prototype testing. Unlike prior general reviews, the specific contributions and structured scope of this work are highlighted as follows:

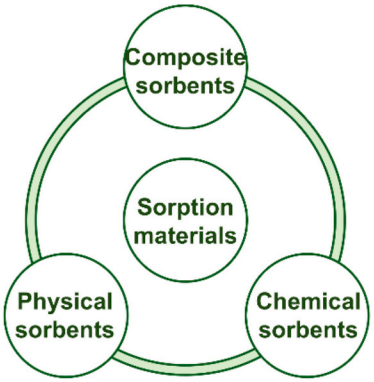
First, the screening criteria and fundamental characterization methodologies for potential adsorbents are systematically introduced to establish a baseline for evaluation. Then, the thermophysical properties and application prospects of state-of-the-art physical, chemical, and composite adsorbents are comprehensively reviewed. Furthermore, representative S-TCES prototypes reported in recent years are categorized and compared to summarize their operational performance under realistic conditions. Finally, and most significantly, leveraging the synthesized dataset, this work provides a quantitative comparison of performance deviations between the material characterization phase and the prototype testing phase. The underlying degradation mechanisms causing these performance losses are unravelled and analysed, concluding with a perspective on future research directions aimed at bridging the gap between material potential and system reality.

Note that in this review, sorption-based thermochemical energy storage refers specifically to reversible sorption/desorption processes developed for the storage and recovery of thermal energy. H_2O is the dominant sorbate in this field, while NH_3 represents the other major working fluid, although its application is more limited because of elevated operating pressure and safety concerns. Gas-sorption processes primarily developed for carbon capture, hydrogen storage, pollutant removal, gas separation, or related purposes are outside the scope of this review.

2. Selection criteria and characterization methods for adsorbents

2.1. Classification of sorption materials for thermal storage

Sorption materials for thermal energy storage can generally be classified into physical sorbents, chemical sorbents, and composite sorbents [64,65], as depicted in Fig. 3. This classification provides a fundamental framework for understanding the performance boundaries and application potential of different adsorbent systems in S-TCES. Physical sorbents, such as porous silica-based materials and activated carbons, store thermal energy mainly through physisorption driven by



Material selection criteria		
High sorption capacity	Good thermal stability	High thermal conductivity
High energy storage density	Sustainability	Non-toxicity
Low charging temperature	Non-corrosiveness	Low cost

Test equipment		Characterization parameters
STA	TG	Weight loss rate, desorption temperature, residual content
	DSC	Heat flow, specific heat, melting point
DVS		Adsorption capacity, isothermal adsorption curve
SEM		Surface morphology, pore structure
XRD		Lattice constants, diffraction peak positions, crystallite size
Climate test chamber		Adsorption capacity, adsorption curve

Fig. 3. Classification, selection criteria, and characterization methods of sorption material.

van der Waals forces [66]. These materials typically exhibit good reversibility and fast response under moderate operating conditions, making them suitable for low- to medium-temperature thermal storage applications (e.g., <150°C). However, their relatively limited sorption enthalpy often constrains the achievable ESD at the prototype level [63]. In contrast, chemical sorbents rely on stronger chemisorption or reversible chemical reactions, enabling significantly higher theoretical energy storage densities. Such materials are attractive for applications requiring compact storage and high ESD, but they often require higher regeneration temperatures (>200°C [67]), slower kinetics, or greater sensitivity to operating conditions, which can challenge practical system integration [63,66].

Composite sorbents have emerged as a hybrid strategy that combines the advantages of both physical and chemical sorbents [68]. By integrating multiple functional components such as porous matrices, salt hydrates, or thermal conductivity-enhancing additives, composite materials aim to balance sorption capacity, thermal stability, and transport properties [68]. As a result, they offer increased flexibility in tailoring material performance to meet specific system requirements. Overall, this classification highlights that no single adsorbent category is universally optimal [39]. Instead, the selection of sorption materials must be guided by a clear understanding of the target application, operating conditions, and prototype-level performance objectives, which are discussed further in the following sections.

2.2. Material selection criteria for S-TCES

The selection of adsorbents for S-TCES is governed by a combination of thermodynamic performance, heat and mass transfer characteristics, and practical engineering constraints. Rather than optimising a single material property, effective adsorbent selection requires a balanced consideration of multiple criteria that collectively determine prototype-level efficiency, reliability, and applicability [69]. From a system perspective, sorption capacity, achievable ESD, and regeneration temperature constitute the primary energy-related criteria [30]. High sorption capacity is essential to maximise the amount of thermal energy stored per unit mass or volume of adsorbent; however, the practically usable ESD depends not only on the maximum uptake but also on the working temperature and humidity ranges under realistic operating conditions [70]. Equally important is the regeneration (charging) temperature, which defines the compatibility of the adsorbent with available heat sources. Adsorbents requiring lower regeneration temperatures are more readily integrated with low-grade thermal inputs, such as solar thermal energy or industrial waste heat, thereby reducing external energy demand and improving overall system efficiency. Consequently, an optimal adsorbent must offer a favourable trade-off between sorption enthalpy and reversibility within the targeted operating window [64].

While high theoretical ESD is desirable, the practical performance of S-TCES is often limited by heat transfer resistance and thermal stability. Many adsorbents exhibit inherently low thermal conductivity, which can significantly constrain charging and discharging rates and lead to non-uniform temperature distributions within the reactor [69]. In addition, thermal stability under repeated cycling is critical to ensure sustained performance over long-term operation. Adsorbents must retain their sorption characteristics and structural integrity when exposed to repeated thermal and moisture variations. Therefore, adequate thermal conductivity and stable behaviour under cyclic conditions are essential prerequisites for translating material-level potential into reliable prototype-level performance. Beyond performance metrics, environmental compatibility, safety, and cost impose decisive constraints on adsorbent selection [71]. Materials intended for building-scale or distributed thermal storage applications must be non-toxic, non-corrosive, and environmentally benign, minimising risks to both system components and end users. Economic viability further requires that adsorbents be derived from readily available raw materials and manufactured through scalable, cost-effective processes. Even materials with excellent inherent performance may be unsuitable for large-scale deployment if their cost or handling requirements outweigh the benefits at the prototype level. As such, sustainability, safety, and affordability must be considered integral components of the material selection process rather than secondary criteria [64,70].

Although S-TCES material selection is inherently multidimensional, ESD remains the most widely reported quantitative metric in the current

literature and is often a primary target of material development. Accordingly, ESD is adopted as the principal metric for the quantitative comparison in this review. Other important criteria, including thermal stability, cyclic regenerability, environmental compatibility, corrosiveness, and cost, are less consistently reported and are frequently described only qualitatively. In many cases, materials with unacceptable stability or safety characteristics are excluded before detailed S-TCES evaluation. Therefore, these criteria are discussed qualitatively rather than subjected to direct cross-literature statistical comparison.

2.3. Characterization methods for adsorbent evaluation

The evaluation of adsorbents for thermal energy storage requires a combination of thermal, sorption, and structural characterisation methods that collectively link material properties to prototype-level performance. Instead of serving as isolated analytical tools, these characterisation techniques provide complementary information that supports the selection criteria discussed in Section 2.2, as shown in Fig. 3. Thermal and thermochemical analyses are essential for assessing the regeneration behaviour, thermal stability, and reversibility of adsorbents. Techniques such as a simultaneous thermal analyzer (STA), including thermogravimetric analysis (TG) and differential scanning calorimetry (DSC), are commonly used to determine desorption temperatures, mass change behaviour, and heat flow associated with adsorption-desorption processes [72]. These measurements provide direct insight into the operating temperature window and thermal durability of adsorbents, which are critical for evaluating their compatibility with available heat sources and long-term cycling conditions. Therefore, thermal characterisation forms the basis for understanding the energetic feasibility of S-TCES.

Sorption characterisation focuses on quantifying the sorption capacity, kinetics, and equilibrium behaviour under controlled environmental conditions. Dynamic vapor sorption (DVS) systems and climate test chambers (also known as humidity chambers) are widely used to obtain sorption isotherms and uptake curves over relevant temperature and humidity ranges. These methods enable evaluation of both equilibrium storage potential and dynamic response, supporting assessment of achievable ESD and charging/discharging rates. Importantly, sorption characterisation under realistic operating conditions is crucial for bridging the gap between material-level measurements and practical system performance [73]. Structural and morphological characterisation techniques, including scanning electron microscopy (SEM) and X-ray diffraction (XRD), are employed to examine the microstructural features and phase stability of adsorbents. Parameters such as pore structure, particle size, and particle integrity directly influence heat and mass transfer behaviour as well as mechanical robustness. By comparing structural features before and after thermal or sorption cycling, these techniques help identify degradation mechanisms and assess long-term material stability. Consequently, structural characterisation plays a key role in verifying whether promising intrinsic properties can be maintained under repeated operational conditions [72,73].

3. Characterization and performance evaluation of adsorbent materials

The thermodynamic performance and operational reliability of an S-TCES system are fundamentally determined by the intrinsic properties of the chosen adsorbent. Consequently, a comprehensive understanding of the material-level characteristics, ranging from equilibrium conditions, adsorbate uptake and binding energy to heat/mass transfer kinetics, is a prerequisite for efficient system design and optimization.

3.1. Review of representative adsorbents

Representative S-TCES adsorbents can be broadly divided into physical, chemical, and composite sorbents. Physical sorbents (e.g., silica gel, zeolite, and MOFs) generally offer good reversibility, relatively low regeneration temperatures, and favorable kinetics, but their storage densities are often moderate. Chemical sorbents can achieve substantially higher storage capacities through reversible hydration/dehydration reactions, although practical limitations such as agglomeration, swelling, deliquescence, and transport deterioration remain important. Composite sorbents combine an active salt with a porous host matrix and are therefore widely investigated as a strategy to balance storage capacity, structural stability, and heat/mass transfer performance. The following discussion compares representative materials from all three categories and examines several composite systems in greater detail to illustrate how material modification affects sorption behavior and ESD. Specifically, this review analyzes how impregnating chemical sorbents into physical host matrices alters key thermophysical parameters. We examine the transition in performance characteristics, such as enhanced sorption capacity and ESD, that occurs when transforming a pure physical adsorbent into a composite material.

To illustrate the performance evolution from a physical matrix to a composite adsorbent, the work conducted by Xu et al. [74] serves as a representative example. In this study, a composite adsorbent, designated as $MgCl_2$@ZEO_22, was synthesized by impregnating a zeolite 13X host matrix with 22 wt% hygroscopic $MgCl_2$. Fig. 4 provides a comprehensive visualization of the structural characterization and performance enhancement realized through this synthesis. As depicted in Fig. 4(a), SEM analysis of the pure zeolite 13X revealed the size of crystal granules ranging from 2 to 5 μm, with a uniform distribution of macropores (0.2-2 μm) situated within the inter-crystalline spaces. Complementary transmission electron microscopy (TEM) further identified numerous ordered microchannels with diameters of 0.3-0.8 nm on the zeolite surface. Crucially, comparative observations of the synthesized MgCl2@ZEO_22 indicate that both the granular morphology and the ordered microchannel structure were well preserved during the composite formation, suggesting that the impregnation process did not compromise the structural integrity of the host matrix. Fig. 4(b) presents the macropore volume and pore-size distribution profiles obtained via an automatic mercury porosimeter. A distinct shift in pore characteristics was observed after impregnation: the volume of macropores smaller than 200 nm decreased from 0.05 cm^3/g to 0.03 cm^3/g, attributed to the partial occupation of these pores by the loaded $MgCl_2$ salt. Conversely, the volume of macropores larger than 200 nm increased from 0.21 cm^3/g to 0.27 cm^3/g, likely due to salt agglomeration or surface-coating effects modifying the inter-particle void spaces.

As a consequence of the modified composition and pore architecture post-synthesis, distinct changes in sorption performance are observed, as depicted in Fig. 4(c) and (d). The quantitative impact of salt loading on sorption capacity is illustrated in Fig. 4(c). Under test conditions of 30°C and 80% RH (relative humidity), the water uptake was evaluated across composites with varying salt mass ratios. The results demonstrate a positive correlation between salt content and water uptake. While the pure physical adsorbent (zeolite 13X) showed a limited capacity of only 0.22 g/g, the composite MgCl2@ZEO_22 achieved a significantly higher uptake of 0.75 g/g, representing more than a threefold increase. Fig. 4 (d) compares the water vapor sorption isotherms of pure zeolite 13X, Zeolite NaMgX, and the composite $MgCl_2$@ZEO_22 at 30°C. The composite $MgCl_2$@ZEO_22 showed substantially higher sorption capacity than both counterparts across the pressure range. This enhancement confirms that the chemisorption and absorption mechanisms contributed by the hygroscopic salt play a dominant role in the total storage capacity.

Zhang et al. [75] developed a series of composite sorbents based on expanded vermiculite (EVM) and $SrBr_2$ specifically for low-temperature thermal energy storage. Fig. 5(a) presents the macroscopic photographs and SEM micrographs of the host matrix. The images reveal that EVM has a characteristic worm-like lamellar structure, with high-magnification views confirming an abundant network of macropores formed by stacking these layers, a topology highly conducive to vapor

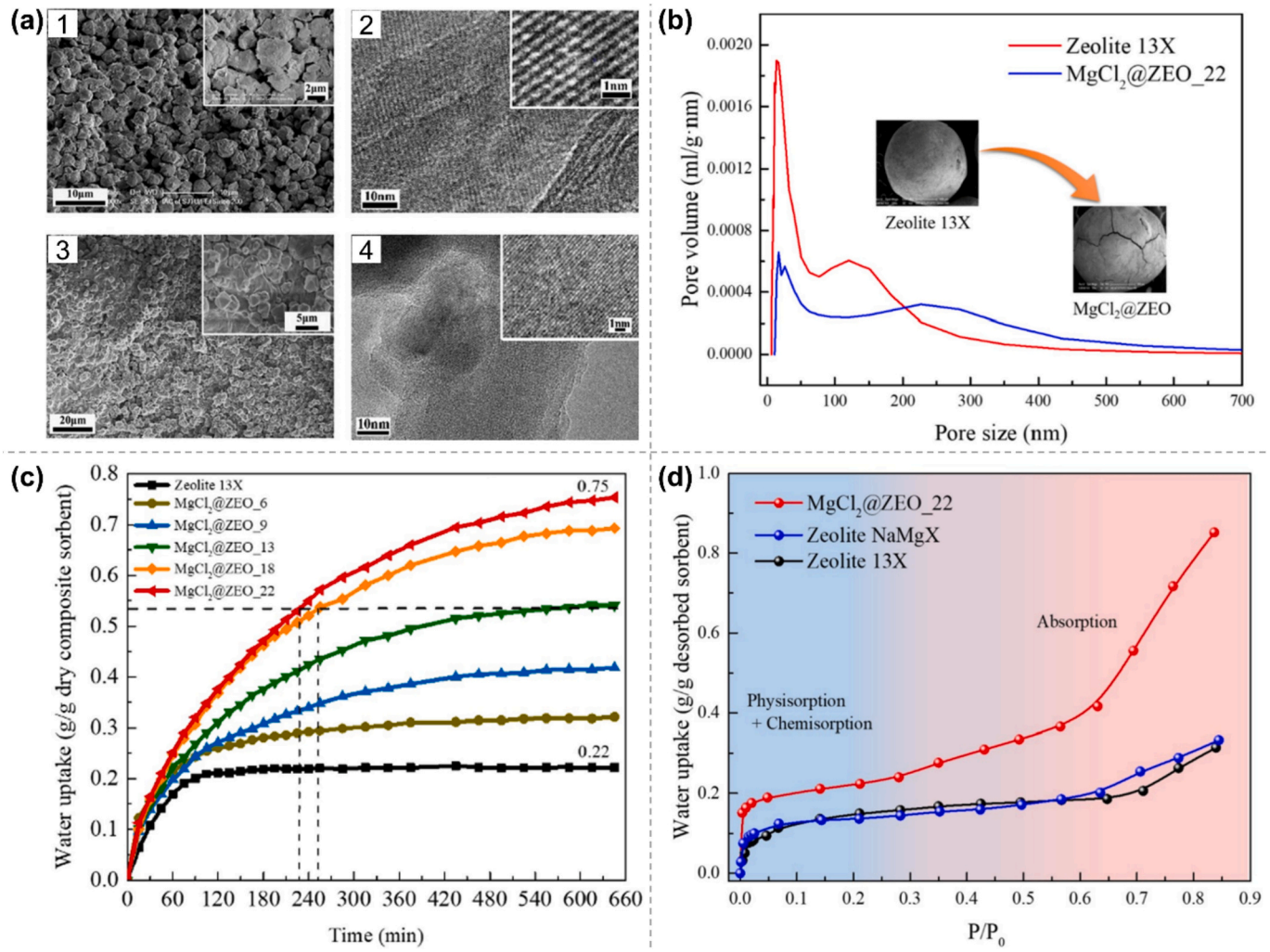


Fig. 4. Structural and sorption characteristics of zeolite 13X and its composite adsorbents: (a) SEM and TEM images: a1) SEM image of zeolite 13X, a2) TEM image of zeolite 13X, a3) SEM image of $MgCl_2$@ZEO_22, a4) TEM image of $MgCl_2$@ZEO_22; (b) macropore diameter distribution of zeolite 13X and $MgCl_2$@ZEO_22; (c) effect of salt content on the water uptake at 30°C and 80% RH; (d) water uptake of sorption isotherm of zeolite 13X, $MgCl_2$@ZEO_22, and zeolite NaMgX composite adsorbent at 30°C. Adapted with permission from Ref. [74], Copyright 2019 Elsevier.

transport. The distribution of $SrBr_2$ within the host matrix is detailed in Fig. 5(b) and (c). SEM observations indicate that the salt hydrates initially tend to nucleate and accumulate in the defect regions of the EVM lamellae. As salt loading increases, the salt progressively coats the entire surface, increasing surface roughness. In the high-loading sample (EVMSrBr$_2$40), the EVM surface is almost entirely encrusted. Notably, this salt accumulation evolves into a "coral-like" architecture, generating a vast number of meso- and micro-pores. This structural transformation significantly augments the specific surface area, thereby maximizing the contact interface available for water vapor interaction.

Fig. 5(d) illustrates the water sorption kinetics for pure EVM, pure $SrBr_2{\cdot}H_2O$, and the composite sorbents. While pure EVM reaches equilibrium rapidly (<30 min), its capacity is negligible (0.03 g/g). In contrast, pure $SrBr_2{\cdot}H_2O$ reaches equilibrium at approximately 150 minutes with a capacity of 0.34 g/g, consistent with the theoretical formation of $SrBr_2{\cdot}6H_2O$. Experimental verification at 30°C and 60% RH confirmed that the reaction remains within the hydration phase without reaching deliquescence. For the composites, water uptake increases significantly but reveals a kinetic trade-off: samples with higher salt loadings require longer durations to reach equilibrium. This phenomenon suggests that as salt fills the porous channels of the EVM, mass transfer resistance intensifies. Specifically, due to this kinetic barrier, the initial uptake rate of the highest loading sample (EVMSrBr$_2$40) was observed to be lower than that of EVMSrBr$_2$30 during the first 120 minutes. Ultimately, at 420 minutes, the specific water uptakes for samples ranging from EVMSrBr$_2$10 to EVMSrBr$_2$40 reached 0.29, 0.42, 0.48, and 0.49 g/g, respectively. The study also highlights the discrepancy between theoretical potential and practical output. Although the theoretical volumetric ESD of $SrBr_2$ is an impressive 496.17 kWh/m^3, the realized performance is often limited by mass-transfer barriers, swelling, and agglomeration. As summarized in Fig. 5(e), while pure EVM contributes a minimal ESD of 2.70 kWh/m^3, the composite sorbents ranging from EVMSrBr$_2$10 to EVMSrBr$_2$40 achieve significantly enhanced ESDs, varying between 38.38 and 105.36 kWh/m^3.

Further exploring the compatibility between inorganic salts and zeolite matrices, Wang et al. [76] conducted a systematic investigation into $MgSO_4$/zeolite 13X composite sorbents. The study evaluated a series of composites with varying salt loadings, designated 13X/5 through 13X/20, using 5 to 20 wt% $MgSO_4$ solutions. Fig. 6 (a) presents the SEM images of the pure matrix and the synthesized composites. The pure zeolite 13X exhibits a well-defined, intricate porous architecture. Upon impregnation, a progressive accumulation of $MgSO_4$ is observed, gradually occupying the internal pore volume. A critical distinction is observed between the 13X/15 and 13X/20 samples, as shown in Fig. 6 (b). The surface of 13X/15 remains relatively clean, whereas the 13X/20 sample exhibits distinct $MgSO_4$ salt crystals exposed on the exterior

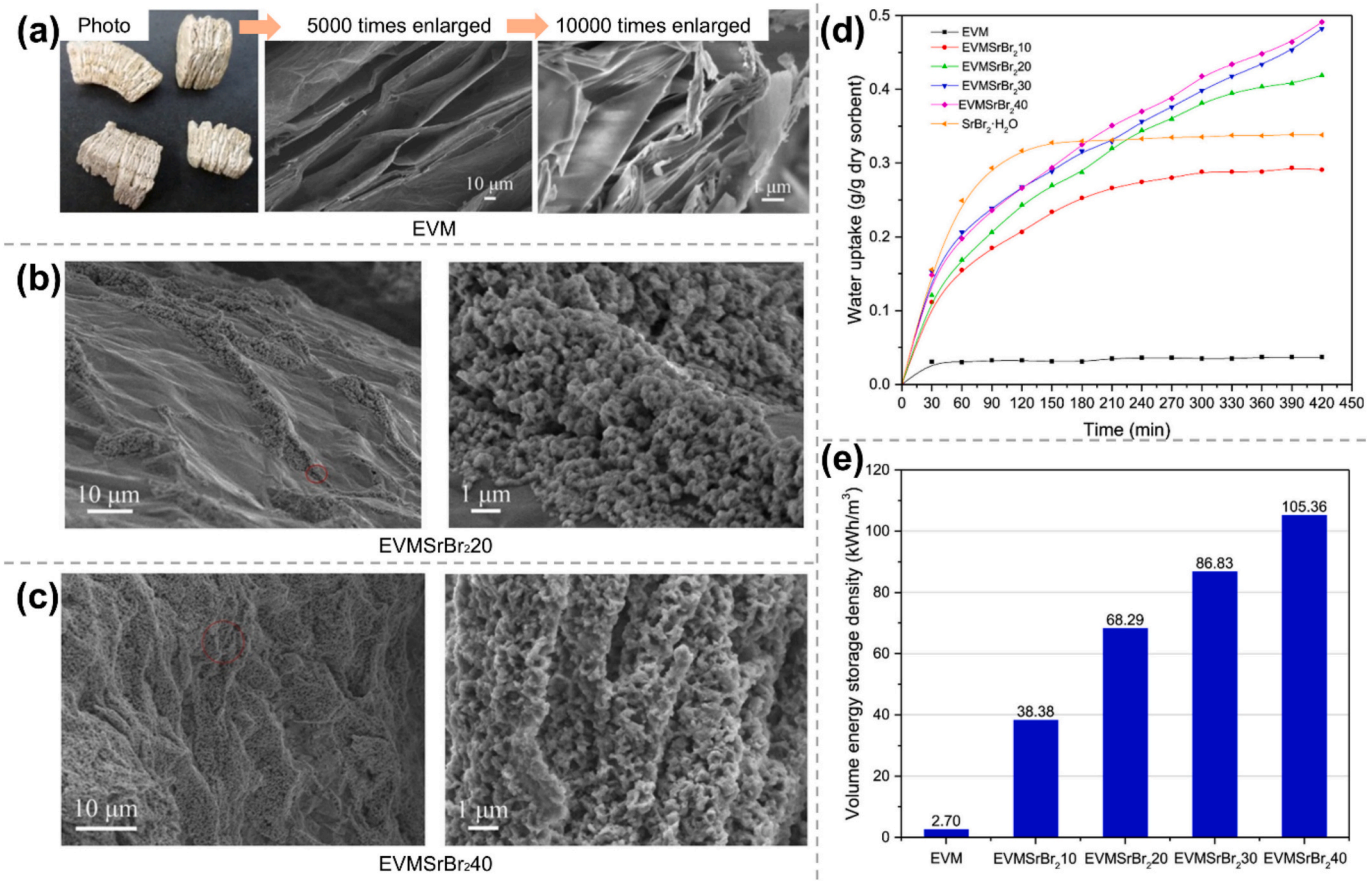


Fig. 5. Microstructural characteristics and sorption performance of EVM and EVM/$SrBr_2$ composite adsorbents: (a) photo and SEM images of EVM, (b) SEM images of EVM/$SrBr_2$20, (c) SEM images of EVM/$SrBr_2$40, (d) water uptake of EVM, $SrBr_2$·H_2O and different EVM/$SrBr_2$ composite adsorbents at 30°C and 60% RH, (e) volumetric ESD of EVM and different EVM/$SrBr_2$ composite adsorbents. Adapted with permission from Ref. [75], Copyright 2016 Elsevier.

surface. This contrast identifies the maximum impregnation capacity of the internal pore network. When the salt loading exceeds this saturation threshold (as in 13X/20), the excess salt crystallizes externally. Consequently, the 13X/20 composite suffers from severe surface agglomeration, rendering it unsuitable for long-term thermal cycling due to potential blockage and structural degradation.

Fig. 6(c) quantifies the mass-specific ESD of the samples under varying humidity conditions. The results demonstrate a universal positive correlation between ESD and RH. For instance, as RH increases from 50% to 80%, the ESD of 13X/15 rises from 530 J/g to 632 J/g, representing a 19% enhancement. Furthermore, at equivalent RH levels, the ESD exhibits a clear upward trend with increasing salt content. Comparative analysis reveals that the 13X/15 composite achieves performance gains of 7%, 9%, 12%, and 14% over the pure zeolite 13X at 50%, 60%, 70%, and 80% RH, respectively. It is noteworthy that this enhancement occurs despite the reduction in specific surface area and pore volume caused by salt impregnation. This indicates that the high hydration enthalpy and strong chemical affinity of $MgSO_4$ for water molecules dominate the storage mechanism, effectively compensating for the loss of physical sorption sites.

To investigate the potential synergistic effects of multi-salt systems, Chen et al. [77] synthesized and characterized a series of vermiculite-based composite adsorbents impregnated with binary and ternary salt mixtures, including V-$CaCl_2$-$MgSO_4$, V-$MgCl_2$-$LiNO_3$, V-$MgSO_4$-LiCl, and V-$MgSO_4$-$LiNO_3$-$MgCl_2$, in which V refers to vermiculite. The microstructural evolution of these composites is presented in Fig. 7(a) via SEM. The pure vermiculite exhibits a characteristic lamellar porous structure, providing ample surface area to accommodate salt hydration. After impregnation, cross-sectional SEM images confirm a significant morphological transformation. The salt mixtures are uniformly embedded throughout the surface and deep within the pores. Fig. 7(b) illustrates the heat flow characteristics derived from DSC measurements. Among the tested samples, the binary V-$CaCl_2$-$MgSO_4$ composite achieved the highest ESD of 1213 kJ/kg. Conversely, the ternary salt mixture (V-$MgSO_4$-$LiNO_3$-$MgCl_2$) failed to obtain the best performance, yielding a lower ESD (774.9 kJ/kg). This reduction is likely due to the dense recrystallization of salts on the vermiculite surface, which may impede sorption kinetics.

The desorption behaviour is further quantified by TG in Fig. 7(c). The V-$CaCl_2$-$MgSO_4$ composite demonstrated superior dehydration kinetics, achieving a maximum mass loss of 58.25% within the 20-150°C range. Specifically, in the low-temperature phase (20-60°C), this composite exhibited a rapid dehydration rate, with a mass loss of ~14% at 60°C, significantly outperforming V-$MgCl_2$-$LiNO_3$ (9%) and the other composites (~7%). By 80°C, the mass loss for V-$CaCl_2$-$MgSO_4$ reached 30%, whereas the ternary mixture only achieved ~15%. The water uptake performance at 45% RH is depicted in Fig. 7(d). V-$CaCl_2$-$MgSO_4$ exhibited the strongest affinity for water vapor, attaining a peak uptake of 0.42 g/g after 20 hours. In contrast, the ternary mixture showed the lowest capacity (0.28 g/g). It is noteworthy that V-$CaCl_2$-$MgSO_4$ showed a relatively low initial uptake rate during the first 0 to 4 hours. This lag phase is attributed to the lamellar structure imposing steric hindrance that initially restricts water-molecule diffusion. However, significant surges in uptake observed at the 4th and 8th hours correspond to the stepwise formation of calcium chloride and magnesium sulfate hydrates, respectively.

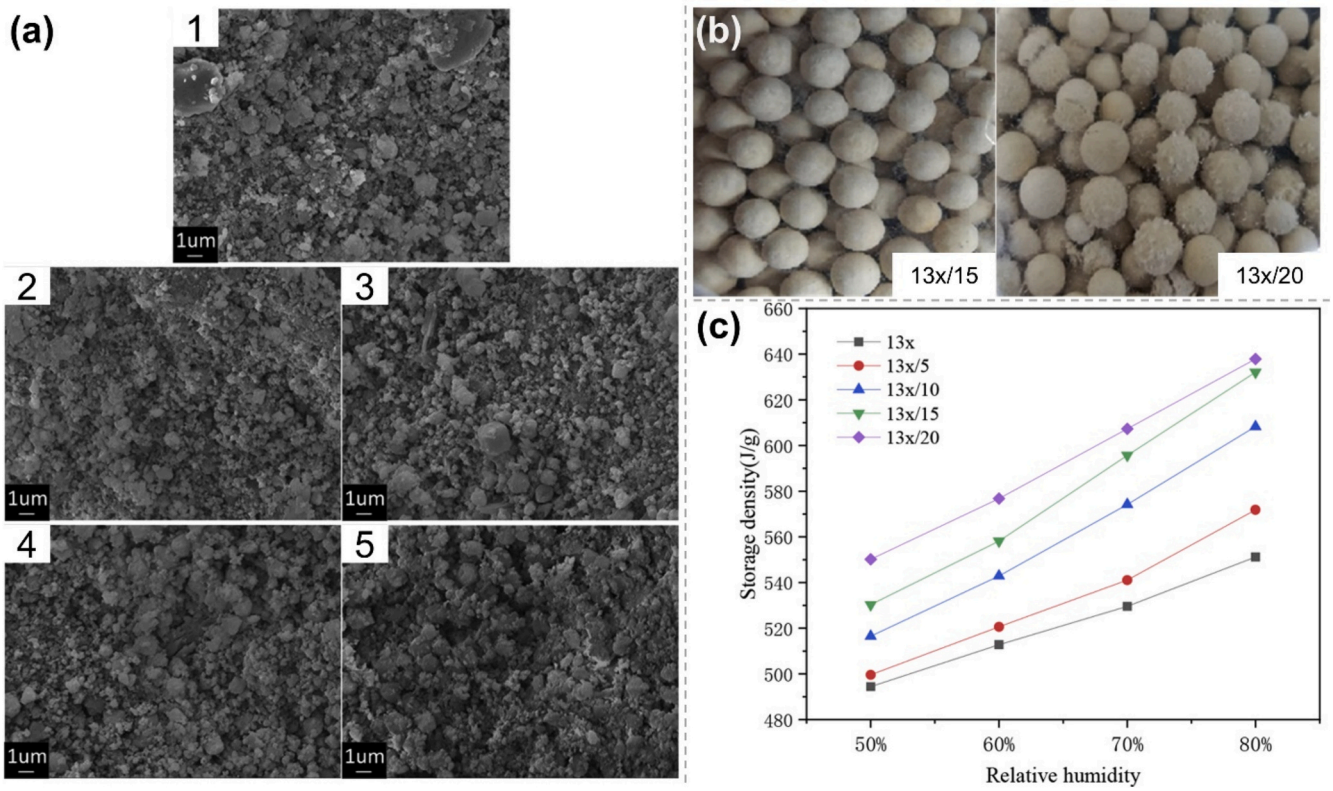


Fig. 6. Morphological and thermal storage properties of zeolite composites: (a) SEM images: a1) zeolite 13X, a2) zeolite 13X/5, a3) zeolite 13X/10, a4) zeolite 13X/15 and a5) zeolite 13X/20, (b) photos of zeolite 13X/15 and zeolite 13X/20, (c) ESD at different RH. Adapted with permission from Ref. [76], Copyright 2019 Elsevier.

3.2. Performance evaluation of adsorbents

Beyond the specific synthesis strategies and optimization mechanisms discussed in the preceding case studies, a holistic evaluation of adsorbent candidates is essential for guiding material selection. However, direct cross-comparison of performance metrics reported in the literature is often complicated by heterogeneous experimental boundary conditions (e.g., regeneration temperature, sorption pressure, and humidity levels) and diverse characterization protocols. To address this challenge and provide a standardized reference, Table 3 presents a comprehensive compilation of data spanning representative physical, chemical, and composite adsorbents. This summary systematically tabulates critical thermodynamic performance indicators, including sorption capacity and mass/volumetric ESD. Crucially, to ensure a rigorous assessment, the table explicitly correlates these performance values with their corresponding measurement methodologies (e.g., STA and DVS) and specific operating conditions. This juxtaposition allows for a more nuanced understanding of the intrinsic capabilities and practical limitations of each material class under realistic operation scenarios.

Physical adsorbents, primarily characterized by porous structures, generally exhibit moderate energy storage capabilities driven by physisorption [101,102]. As shown in Table 3, silica gels typically show specific ESD ranging from 63.4 J/g to 155 J/g. Zeolites, particularly zeolite 13X, show superior performance among traditional physical adsorbents. Under specific conditions (t_g=130°C), zeolite 13X achieved a mass ESD of 921 J/g and a volumetric ESD of 170 kWh/m^3. Emerging MOFs, such as MIP-200 (a zirconium-based metal–organic framework (MOF)) and materials of Institute Lavoisier frameworks-160 (MIL-160), also display competitive properties, with MIP-200 achieving an ESD of 680.4 J/g (220 kWh/m^3) at a relatively low regeneration temperature of 70°C, highlighting their potential for low-grade heat utilization.

Pure chemical adsorbents (salt hydrates) exhibit significantly higher theoretical ESD than their physical counterparts because of the high enthalpy of hydration. Table 3 indicates that $SrBr_2$ is a standout candidate, achieving a remarkable ESD of 1306.86 J/g when tested via STA at a regeneration temperature of 97.4°C. Similarly, $MgSO_4$ demonstrates high potential, with ESD values reaching up to 1309.5 J/g under optimal conditions. However, the data also reflects the sensitivity of these materials to operating conditions; for example, the ESD of $MgCl_2$ varies drastically from 84 J/g to 603 J/g depending on the specific temperature and humidity settings in climate chamber tests.

Composite adsorbents, designed to encapsulate salt hydrates within physical matrices, effectively bridge the performance gap. Expanded natural graphite treated with sulfuric acid (ENG-TSA) is also often incorporated into the adsorbent to increase thermal conductivity. The data confirm that composites generally surpass pure physical adsorbents while mitigating the practical issues of pure salts. Vermiculite-based composites demonstrate exceptional performance. Notably, the LiCl/Vermiculite composite achieved one of the highest reported ESD values of 1880 J/g, and the $SrBr_2$/Expanded vermiculite composite reached 1540.65 J/g. Zeolite-based composites also show substantial improvements. More meaningful evidence is provided by studies comparing reference and modified materials under identical operating conditions. For example, $MgCl_2$@ZEO_22 exhibited a water uptake of 0.75 g/g at 30°C and 80% RH, compared with 0.22 g/g for pure zeolite 13X [74]. Similarly, $MgSO_4$/zeolite 13X showed 7–14% higher ESD than pure zeolite 13X over an RH range of 50–80% under otherwise identical test conditions [76]. Multi-salt composites, such as the Vermiculite-based ternary system ($MgSO_4$/$CaCl_2$/Vermiculite), achieved ESDs in the range of 1108-1213 J/g, validating the efficacy of multi-component salt optimization. In summary, while physical adsorbents offer stability at lower capacities, pure salts offer high capacity with stability risks. These controlled comparisons demonstrate that salt impregnation can enhance sorption capacity or ESD at the material level. However, whether these

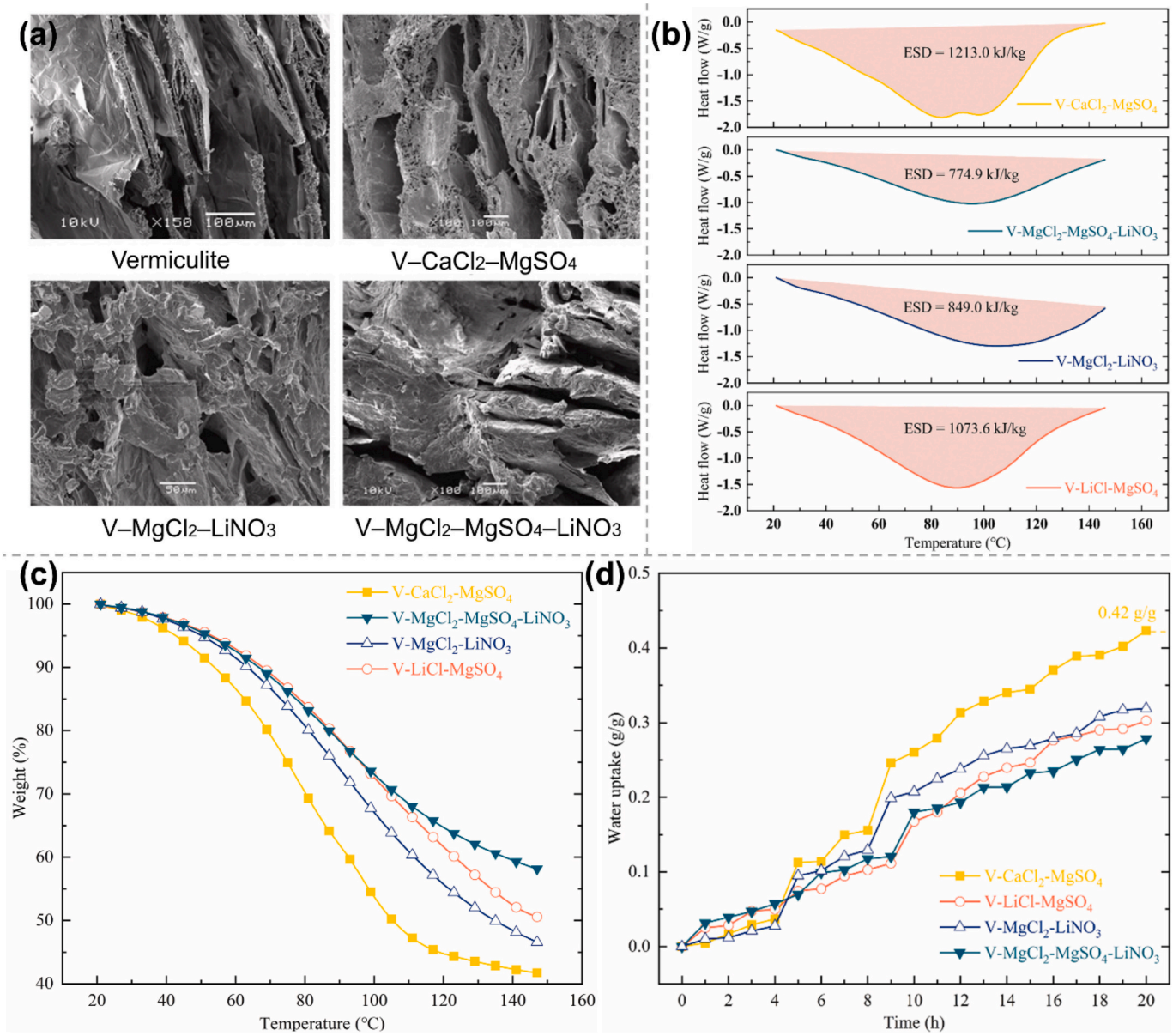


Fig. 7. Physicochemical characterization and hygroscopic performance of vermiculite-based salt mixture composites: (a) SEM images, (b) DSC results, (c) TG results, (d) water uptake. Adapted with permission from Ref. [77], Copyright 2023 Elsevier.

gains are retained after material shaping and reactor integration remains insufficiently demonstrated. Composite sorbents should therefore be regarded as promising, rather than universally superior, candidates for practical S-TCES.

4. Prototype testing and operational performance of S-TCES systems

The transition from laboratory-scale material characterization to prototype-level operation represents a critical leap in S-TCES technology development. While the thermophysical properties of adsorbents determine the theoretical upper limit of energy storage performance, the realized performance of an S-TCES system is equally governed by reactor design, heat exchanger configuration, and dynamic operational strategies. Upon scaling up from milligram-level samples to kilogram-scale packed beds, complex transport phenomena emerge as dominant constraints. A key intermediate step in this transition is shaping sorbent powders and assembling them into packed beds. Pelletization, binder addition, and compaction are often required to improve mechanical stability and packing density. However, these processes introduce inherent trade-offs. Higher compaction may improve volumetric loading and effective thermal conductivity, but can reduce bed permeability and increase vapor diffusion resistance. Similarly, binders can enhance mechanical strength while decreasing the active sorbent fraction and potentially blocking transport pathways. Therefore, part of the material-to-prototype performance gap may originate at the shaped-material and packed-bed scales, prior to additional reactor-level losses associated with heat exchangers, flow maldistribution, and heat loss. Therefore, evaluating S-TCES technology solely based on material isotherms is insufficient. This section critically reviews representative S-TCES prototypes developed in recent years. By categorizing them as open or closed systems, we analyze their structural innovations and quantify key performance metrics, including ESD and ESE, under realistic operating conditions. This analysis aims to identify the engineering bottlenecks that currently hinder the full exploitation of high-performance composite adsorbents.

Table 3
Summary of sorption performance for representative physical, chemical, and composite adsorbents.

Adsorbent	Adsorbate	Test equipment	Sorption performance							Ref.
			Operating condition				Sorption capacity	Energy storage density		
			Desorption		Adsorption					
			t_g (°C)	t_c (°C)/*RH* (%)	t_a (°C)	t_e (°C)/RH (%)	(g/g)	(J/g)	(kWh/m^3)	
Physical adsorbents										
Silica gel	H_2O	ASAP2020 gas adsorption analyzer	80	35	35	15	–	63.4	–	[78]
Silica gel	H_2O	–	90	40	40	15	–	126.0	–	[79]
Silica gel	H_2O	–	160	40	40	15	–	86.4	–	[79]
Silica gel	H_2O	DVS	75	15	35	5	0.059	155.12		[80]
Silica gel	H_2O	–	140	–	30	46.6%	–	–	141	[81]
Silica gel	ethanol	DVS	75	15	35	5	0.025	24.84	–	[80]
Silica gel	H_2O	STA	200	–	–	–	0.11	479.4	–	[82]
Zeolite	H_2O	STA	274	21/34%	–	–	0.131	141	50	[83]
Zeolite 4A	H_2O	–	140	–	30	46.6%	–	–	132	[81]
Zeolite 13X	H_2O	–	140	–	30	46.6%	–	–	179	[81]
Zeolite 13X	H_2O	–	150	–	25	80%	–	551	–	[76]
Zeolite 13X	H_2O	–	130	–	12	75%	0.30	921	170	[84]
Expanded vermiculite	H_2O	STA	70.4	–	30	60%	0.03	75.96	–	[75]
MIP-200	H_2O	–	70	30	30	10/35%	0.39	680.4	220	[85]
MIL-160	H_2O	–	70	30	30	10/35%	0.35	388.8	115	[85]
CAU-10	H_2O	–	70	30	30	10/35%	0.30	238	274	[85]
SAPO-34	H_2O	–	70	30	30	10/35%	0.29	414	165	[85]
MOF-801	H_2O	–	70	30	30	10/35%	0.28	370.8	163	[85]
Chemical adsorbents										
$CaCl_2$	H_2O	STA	190	21/34%	–	–	0.611	801	408.3	[83]
$CaCl_2$	H_2O	TG	146	–	25	30%	–	–	583	[86]
$SrBr_2$	H_2O	STA	97.4	–	30	60%	0.34	1306.86	–	[75]
$SrBr_2$	H_2O	STA	120	–	30	40%	0.44	–	–	[87]
$SrBr_2$	H_2O	Climate test chamber	90	–	30	43%	0.345		–	[87]
$SrBr_2$	H_2O	–	256	–	–	–	–	291	102	[43]
$SrBr_2$	H_2O	Climate test chamber	100	–	20	65%	–	902	598	[88]
$SrCl_2$	H_2O	TG	128	–	25	71%	–	–	667	[86]
$SrCl_2$	H_2O	Climate test chamber	140	–	22	65%	–	1334	715	[88]
$SrCl_2$	H_2O	Climate test chamber	100	–	22	65%	–	1110	595	[88]
$SrCl_2$	H_2O	Climate test chamber	70	–	22	65%	–	955	512	[88]
$MgSO_4$	H_2O	TG	>230	–	25	90%	–	–	583	[86]
$MgSO_4$	H_2O	Climate test chamber	140	–	22	65%	–	1204	562	[88]
$MgSO_4$	H_2O	Climate test chamber	100	–	22	65%	–	991	463	[88]
$MgSO_4$	H_2O	Climate test chamber	70	–	22	65%	–	630	294	[88]
$MgSO_4$	H_2O	STA	150	25/40%	–	–	–	1309.5	611.1	[89]
$MgSO_4$	H_2O	STA	150	–	25	–	–	452.4	211.1	[89]
$MgCl_2$	H_2O	TG	230	–	25	33%	–	–	555	[86]
$MgCl_2$	H_2O	Climate test chamber	140	–	22	65%	–	603	261	[88]
$MgCl_2$	H_2O	Climate test chamber	100	–	22	65%	–	246	107	[88]
$MgCl_2$	H_2O	Climate test chamber	70	–	22	65%	–	84	37	[88]
$MgCl_2$	H_2O	STA	104	1.5%	61	5.3%	–	–	536.1	[90]
Na_3PO_4	H_2O	Climate test chamber	140	–	22	65%	–	1162	523	[88]
Na_3PO_4	H_2O	Climate test chamber	100	–	22	65%	–	1194	537	[88]
Na_3PO_4	H_2O	Climate test chamber	70	–	22	65%	–	1120	504	[88]
$Al_2(SO_4)_3$	H_2O	TG	>300	–	25	–	–	–	444	[86]
APO-Tric	H_2O	STA	95	–	40	–	0.318	947	240	[91]
$CuCl_2$	H_2O	Nuclear Magnetic Resonance	150	–	30	66%	–		333.3	[92]
Na_2S	H_2O	STA	82	3.6%	66	4.2%	–	–	775	[90]
K_2CO_3	H_2O	STA	65	7.6%	59	5.8%	–	–	361.1	[90]
K_2CO_3	H_2O	–	100	–	25	–	–	–	222.2	[90]
Composite adsorbents										
$CaCl_2$ (30%)/Silica gel	H_2O	STA	85	15	30	10	0.325	887.77	–	[93]
LiCl (30%)/Silica gel	H_2O	DVS vacuum analyser	95	–	30	–	0.6	335	–	[94]
LiCl (30%)/Silica gel	H_2O	ASAP2020 gas adsorption analyzer	80	35	35	15	–	607.3	–	[78]
$MgSO_4$ (30%)/Silica gel	H_2O	STA	150	–	–	–	–	792.9	–	[82]
$CuSO_4$ (30%)/Silica gel	H_2O	STA	245	–	–	–	–	580.5	–	[82]
$Al_2(SO_4)_3$ (30%)/Silica gel	H_2O	STA	200	–	–	–	–	712.6	–	[82]
LiCl (52%) /Vermiculite	H_2O	STA	85	30	35	10	–	1880	–	[95]
$SrBr_2$ (94%)/ENG-TSA	H_2O	STA	–	–	30	40%	0.415	–	–	[87]
$SrBr_2$ (40%)/Expanded vermiculite	H_2O	STA	96.1	–	30	60%	0.53	1540.65	–	[75]
$SrBr_2$/Silica gel	H_2O	STA	80	2.3%	30	28.9%	0.22	–	203	[96]

(*continued on next page*)

Table 3 (*continued*)

Adsorbent	Adsorbate	Test equipment	Sorption performance							Ref.
			Operating condition				Sorption capacity	Energy storage density		
			Desorption		Adsorption					
			t_g (°C)	t_c (°C)/*RH* (%)	t_a (°C)	t_e (°C)/RH (%)	(g/g)	(J/g)	(kWh/m^3)	
$CaCl_2$/Vermiculite	H_2O	–	150	–	20	80%	1.41	–	290	[97]
$SrCl_2$ (50%)/Cement	H_2O	–	130		12	75%	0.28	880	145	[84]
$MgSO_4$ (15%)/Zeolite 13X	H_2O	Calvet calorimetric cell	150	30/50%	–	–	–	648	166	[98]
$MgSO_4$ (15%)/Zeolite 13X	H_2O	–	150	–	25	80%	–	632	–	[76]
$MgSO_4$ (15%)/Zeolite 13X/ ENG-TSA	H_2O	STA	200	–	–	–	0.205	635.84	–	[99]
$MgSO_4$ (16.5%)/Activated alumina	H_2O	STA	200	–	–	–	0.118	425.86	–	[99]
$MgCl_2$/Zeolite 13X	H_2O	–	140	–	30	46.6%	–	–	272	[81]
$MgCl_2$ (22%)/Zeolite 13X	H_2O	STA	200	30	30	80%	0.55	1558	–	[74]
$MgCO_3$ (50%)/Silica gel	H_2O	–	–	–	25	100%	0.26	410	–	[100]
$MgCO_3$ (50%)/Silica gel	H_2O	–	–	–	5	90–100%	0.15	290	–	[100]
$MgSO_4$ (18.4%)/$CaCl_2$ (36.8%)/Vermiculite	H_2O	STA	150	–	–	–	0.51–0.58	1108–1213.0	–	[77]

4.1. Open S-TCES systems

Open S-TCES systems are characterized by their mechanical simplicity, as they operate at atmospheric pressure without the stringent requirement for hermetic sealing. In this configuration, the working fluid, typically ambient air, is in direct contact with the adsorbent material. The most conventional implementation is the single-layer packed bed, as illustrated in Fig. 8(a) [77]. In this setup, the adsorbent is encapsulated within a singular flat layer. An external fan drives airflow through this porous medium, facilitating the heat and mass transfer needed for charging and discharging. However, this topology faces significant limitations during upscaling. To increase energy storage capacity, the cross-sectional area (length and width) of the single layer must be expanded proportionally. This expansion inevitably leads to excessive footprints and unwieldy form factors, requiring oversized auxiliary components (e.g., ducts and manifolds). Consequently, the resulting poor volumetric compactness renders large-scale single-layer systems impractical for many engineering applications where space is a constraint.

To overcome these geometric limitations and enhance system integration, multi-layer configurations have been proposed, as depicted in Fig. 8(b), (c), and (d). The first multi-layer configuration (Fig. 8(b)) employs a stacked or parallel arrangement of multiple adsorbent layers [103]. By distributing the adsorbent across several distinct layers, the system significantly improves its compactness and design flexibility. The airflow is directed to traverse the adsorbent layers, ensuring sufficient contact time and reactive surface area while maintaining a manageable equipment footprint. This structural optimization effectively reconciles the trade-off between high storage capacity and compact system volume [106,107]. Moreover, Fig. 8(c) illustrates a multi-layer series arrangement [49], which is conceptually analogous to folding a large single bed into a compact volume. In this design, the layers feature alternating openings along the airflow direction. Air enters the inter-layer plenum and diffuses bidirectionally, i.e., penetrating both the upper and lower adjacent adsorbent layers, before exiting. This topology not only maximizes the volumetric energy density but also ensures a uniform flow distribution within a compact footprint [48]. Alternatively, Fig. 8(d) presents a cylindrical module design [104]. The adsorbent is packed into hollow cylinders featuring a central air channel sealed at the top end (by adsorbent). When arranged in a parallel array, the airflow is forced from the bottom upwards into the central cavities and then radially outward through the porous walls. This radial flow geometry substantially increases the specific contact surface area relative to the bed volume, thereby accelerating the overall reaction kinetics.

To overcome the mass-transfer limitations inherent in fixed beds, Fig. 8(e) and (f) introduce dynamic reactor concepts. These designs mobilize the solid adsorbent to maximize gas-solid contact and achieve dynamic interaction. As shown in Fig. 8(e), this system utilizes a gravity-feed mechanism [42]. The bulk adsorbent is stored in an upper hopper and discharged through a narrow, elongated slit into a flat vertical channel. As the particles descend under gravity, a cross-flow air stream passes through the falling "curtain" of adsorbent, ensuring thorough reaction. Upon accumulating in the bottom collection vessel, the material is mechanically hoisted back to the upper hopper for subsequent cycles. Fig. 8(f) employs a vibration-assisted mechanism [105]. The adsorbent is dispensed onto a sieve subjected to mechanical vibration, which disperses the material into an agitated granular state. Simultaneously, an upward airflow passes through the sieve, interacting intimately with the suspended particles before they settle into a receiver tank. These dynamic designs offer significant operational advantages: they markedly enhance adsorption reaction rates and effectively mitigate the risk of particle agglomeration, a common failure mode in static beds. Furthermore, the rate of energy release can be actively controlled by modulating the mass flow rate of the solid adsorbent, allowing precise load matching to user demand. However, these enhancements incur notable penalties: the introduction of moving parts increases initial capital expenditure and maintenance requirements, while mechanical actuation raises the system's parasitic energy consumption. Additionally, the need for hoists, vibrators, and collection tanks typically results in a bulky system footprint, rendering these designs less suitable for space-constrained applications.

4.2. Closed S-TCES systems

In contrast to open systems, closed S-TCES systems operate under fundamentally different thermodynamic principles. Open systems use ambient air as a dual-purpose medium, acting as both the adsorbate (moisture) carrier and the direct heat transfer fluid (HTF). Closed S-TCES systems operate in isolation from the atmosphere and therefore require hermetic containment and removal of non-condensable gases. However, their operating-pressure regime depends strongly on the working pair. Water-based adsorption systems generally operate at sub-atmospheric vapor pressures and thus require vacuum-tight vessels. In contrast, ammonia-based systems may operate at several bars or higher, depending on the refrigerant temperature and sorption equilibrium. In salt-salt resorption systems, the operating pressure is governed by the equilibrium pressures of the two coupled sorption reactions and is not inherently sub-atmospheric. In the closed configuration, the adsorbate (refrigerant) is hermetically contained within the system and stored in a liquid state in a separate reservoir. Moreover, heat transfer is decoupled

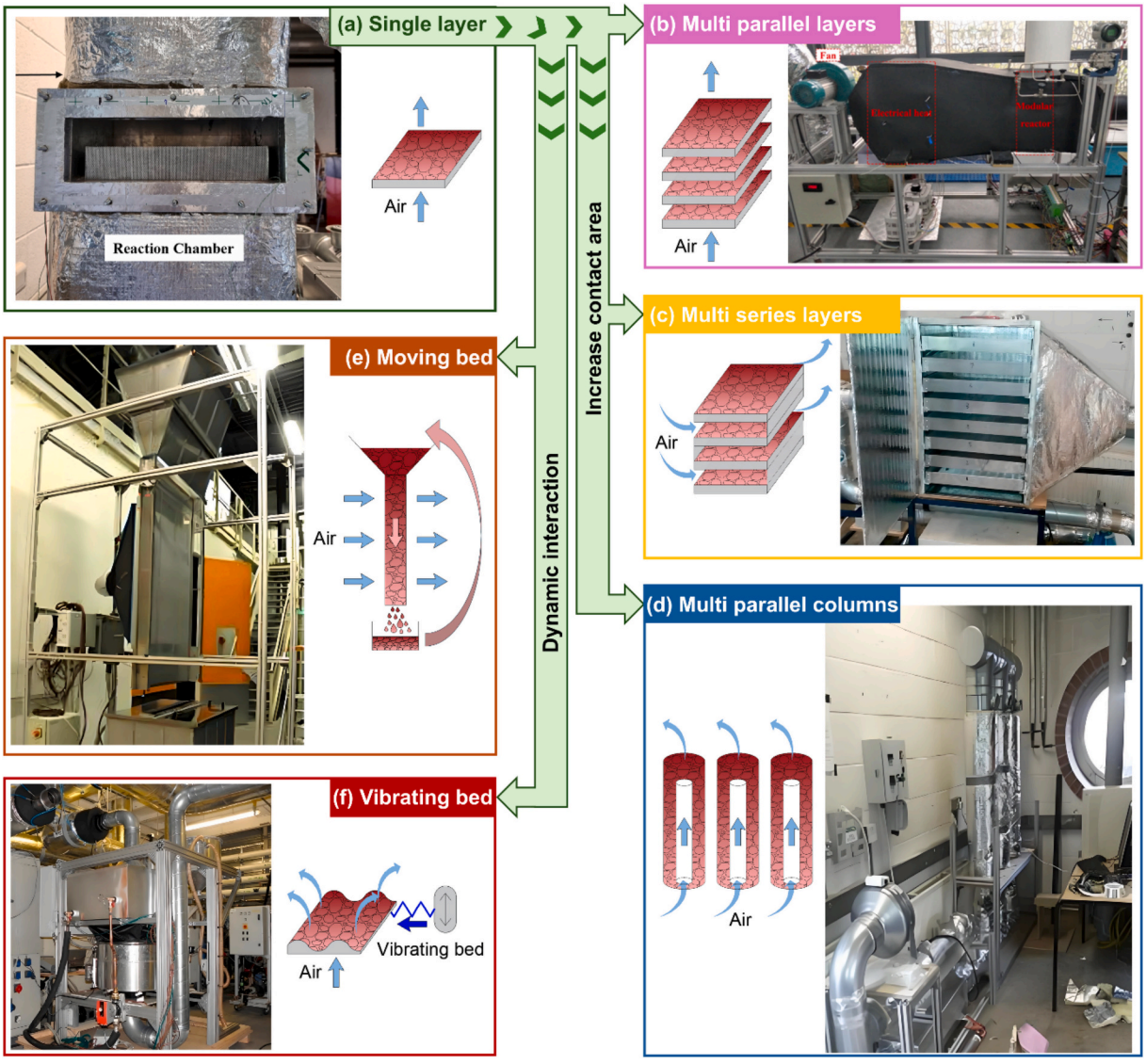


Fig. 8. Reactor designs for open S-TCES prototype: (a) single-layer reactor, adapted with permission from Ref. [77], Copyright 2023 Elsevier; (b) multi-parallel-layer reactor, adapted with permission from Ref. [103], Copyright 2017 Elsevier; (c) multi-series-layer reactor, adapted with permission from Ref. [49], Copyright 2018 Elsevier; (d) multi-parallel-column reactor, adapted with permission from Ref. [104], Copyright 2016 Elsevier; (e) moving-bed reactor, adapted with permission from Ref. [42], Copyright 2019 Elsevier; (f) vibrating reactor, adapted with permission from Ref. [105], Copyright 2018 Elsevier.

from mass transfer: thermal energy is supplied to or extracted from the adsorbent bed via indirect heat exchange. This is typically realized by integrating heat exchanger coils within the adsorbent bed, through which an HTF (usually water or thermal oil) circulates. The heat exchange occurs across the coil walls, preventing direct contact between the HTF and the adsorbent.

Hermetic operation nevertheless imposes additional constraints on reactor design. Moving or vibrating beds are not fundamentally excluded from closed systems, but their implementation introduces greater challenges in maintaining leak-tight pressure containment and integrating moving solids with internal heat exchangers. These constraints are particularly associated with vacuum integrity in water-based systems and pressure-resistant sealing in ammonia-based systems. Consequently, most reported closed S-TCES prototypes employ static packed-bed configurations, although this represents a practical design preference rather than an intrinsic thermodynamic requirement. Research efforts are primarily directed toward two vectors: 1) maximizing the contact interface between the adsorbent and the vaporized refrigerant, 2) optimizing the heat exchange between the adsorbent and the HTF circulating in the coils.

Fig. 9 presents a comparative overview of the closed-system designs, illustrating a typical packed-bed configuration (Fig. 9(a)) alongside three advanced layout modifications designed to address heat and mass transfer limitations (Fig. 9(b), (c), and (d)). For small-scale devices and early-stage experimental prototypes, the single-layer adsorbent bed with embedded heat exchange coils remains the classical approach, as depicted in Fig. 9(a) [95]. In this configuration, the adsorbent material is packed in a monolithic layer around the HTF tubes. While effective for fundamental studies, this layout faces significant scaling challenges. As reactor volume increases, the thicker adsorbent bed leads to excessive thermal and diffusion resistance.

To overcome the limitations of bulk-packed beds, closed systems adopt strategies similar to those used in open configurations to maximize the contact interface between the solid adsorbent and the vaporized refrigerant. Fig. 9(b) illustrates a multilayer arrangement in which the adsorbent is divided into thinner segments [108]. This configuration reduces the characteristic diffusion length, thereby accelerating the adsorption kinetics. As shown in Fig. 9(c), integrating dedicated vapor

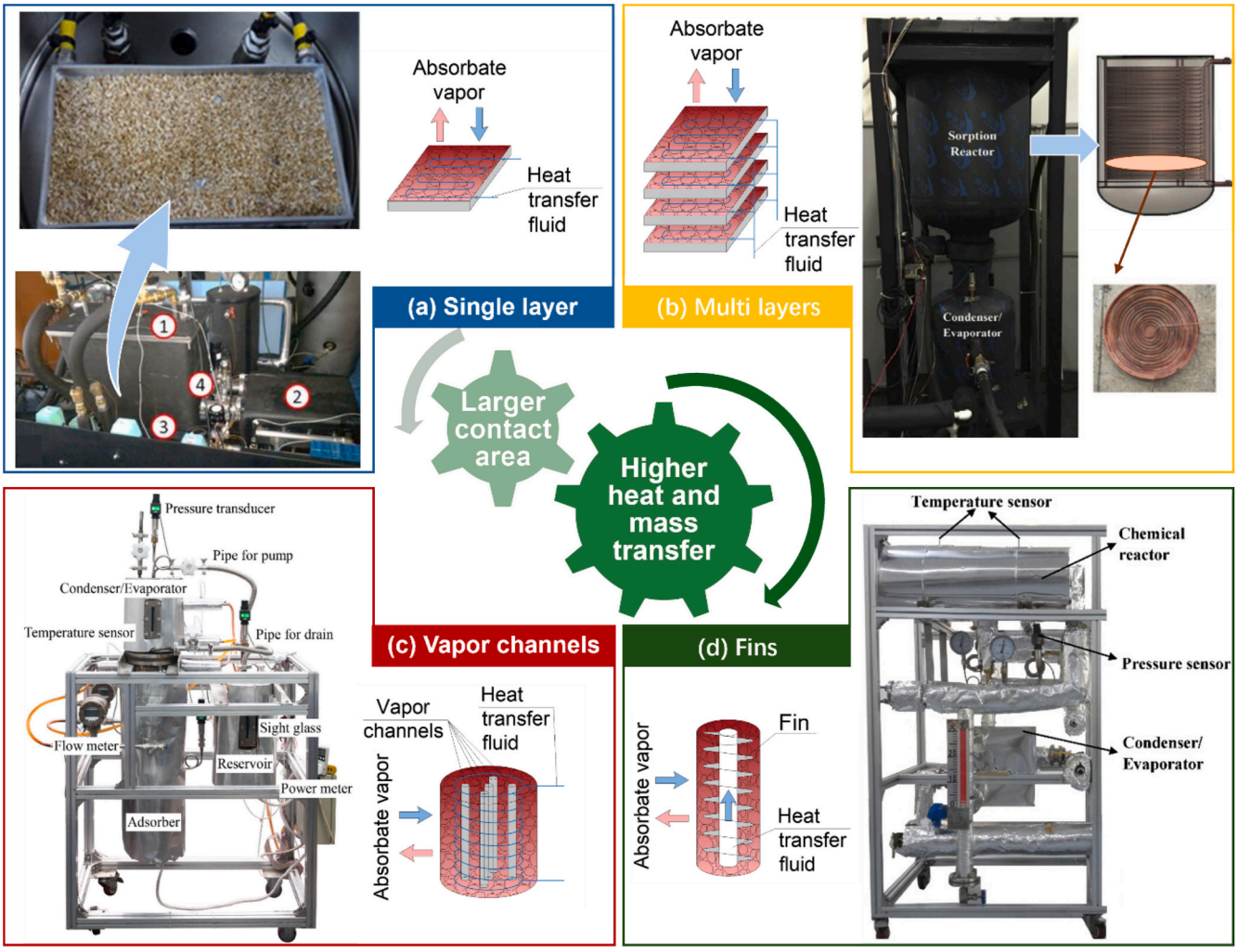


Fig. 9. Reactor designs for closed S-TCES prototypes: (a) single-layer reactor, adapted with permission from Ref. [95], Copyright 2019 Elsevier; (b) multi-layer embedded reactor, adapted with permission from Ref. [108], Copyright 2016 Elsevier; (c) additional mass-transfer channels reactor, adapted with permission from Ref. [99], Copyright 2019 Elsevier; (d) fin-enhanced column reactor, adapted with permission from Ref. [109], Copyright 2023 Elsevier.

distribution channels allows more uniform penetration of the adsorbate into the core of the bed [99,110]. By increasing the effective reaction area per unit volume, these designs significantly enhance the volumetric adsorption and desorption rates.

Alternatively, research has focused on intensifying the thermal coupling between the adsorbent and the HTF to improve system heat flux. Fig. 9(d) presents a cylindrical adsorbent module with a central heat exchange tube [109,111,112]. To compensate for the low thermal conductivity of the adsorbent material, the HTF tube is equipped with extended surfaces or fins. These fins may take various geometric forms, including spiral, annular [113], Y-shaped [114], or dendritic (tree-like) shapes, to distribute heat effectively throughout the radial depth of the adsorbent. While the addition of fins significantly reduces thermal resistance, it simultaneously creates a more tortuous path for vapor flow, increasing mass-transfer resistance. Consequently, the optimization of fin length, spacing, and morphology is a critical research area, aimed at finding the ideal equilibrium between enhanced heat transfer and minimized pressure drop within the adsorbent matrix.

4.3. Performance evaluation of S-TCES prototypes

Table 4 provides a comprehensive summary of the storage performance for representative S-TCES prototypes, categorizing them by adsorbent-adsorbate pairs, reactor configurations, and operational boundary conditions. This comparison elucidates the transition from material-level potential to prototype-level realization across various open and closed configurations. It should be noted that all volumetric ESD values used for the cross-scale comparison in this review are based on the volume of the sorption material, rather than the packed-bed, reactor, or total system volume. This consistent basis is adopted to enable comparison between material-level characterization and prototype-level measurements. The choice of reactor configuration involves inherent trade-offs rather than a single universally superior design. Conventional fixed or packed beds offer structural simplicity but may suffer from increasing heat/mass-transfer resistance and flow maldistribution as bed size increases. Multi-layer configurations reduce characteristic diffusion lengths and improve vapor or airflow distribution, thereby enhancing dynamic sorption rates, but require more complex manifolds and internal structures. Moving and vibrating beds can continuously renew the gas–solid contact interface and alleviate local transport limitations, whereas their mechanical complexity and auxiliary energy consumption may offset part of the performance benefit. At present, however, quantitative comparison among these configurations remains difficult because the reported prototypes employ different working pairs, operating conditions, system scales, and performance definitions. Therefore, the values summarized in Table 4 should be interpreted as representative system performance rather than as a direct ranking of reactor designs.

Table 4
Summary of the storage performance for representative prototypes.

Adsorbent	Adsorbate	Operating condition				Reactor type	Energy storage efficiency (–)	Energy storage density		Ref.
		Charging		Discharging						
		t_g (°C)	t_c (°C) /RH (%)	t_a (°C)	t_e (°C) /RH (%)			J/g	kWh/m^3	
Open system										
Silica gel	H_2O	120	0–3%	22	90%	Packed column	–	–	200.7	[115]
Zeolite 13X	H_2O	150	–	25	50%	Packed column	–	430	121	[116]
Zeolite 13X	H_2O	150	–	19–20	60–70%	Packed column	0.66	–	164	[117]
$MgCl_2$ (35%)/Coral aggregate	H_2O	150	–	25	50%	Packed column	–	260.75	74.25	[116]
$SrCl_2$ (25%)/Al_2O_3	H_2O	150	–	20	70%	Packed column	–	611.7	150.5	[118]
$SrCl_2$ (10%)/Silica gel	H_2O	80	–	25	70%	Packed column	–	724	100	[107]
$SrCl_2$ (35%)/Cement	H_2O	150	–	19–20	60–70%	Packed column	0.55	448	96	[117]
$SrCl_2$ (50%)/Cement	H_2O	150	–	19–20	60–70%	Packed column	0.60	629	136	[117]
$CaCl_2$/Vermiculite	H_2O	80	37.7%	21	75%	Packed column	0.61–0.69	–	290	[104]
$CaCl_2$ (40%)/Silica gel	H_2O	60	–	22.6	40%	Vibrating bed	–	576	–	[105]
$CaCl_2$ (40%)/Silica gel	H_2O	85	–	22.6	40%	Vibrating bed	–	720	–	[105]
$SrBr_2$	H_2O	80	–	25	31%	Multi–layer packed bed	–	1130.4	–	[41]
$MgSO_4$ (18.4%)/$CaCl_2$ (36.8%)/Vermiculite	H_2O	120	–	17–19	70–80%	Packed bed	–	–	161.01–197.34	[77]
$MgSO_4$ (20%)/Silica gel	H_2O	110–130	–	30–50	80%	Fixed bed	0.656	381.36	–	[119]
$MgCl_2$	H_2O	130	–	51	8.8%	Packed column	–	1947.6	–	[120]
Closed system										
Zeolites	H_2O	180	17	45	20	Packed column	–	–	150	[121]
LiCl (40%)/AC/ENG-TSA/ Silica gel	H_2O	85	15	40	15	Packed bed	0.93	874	–	[122]
LiCl (93.6%)/ENG	H_2O	85	18	40	18	Packed bed	0.56	1761.9	–	[108]
$CaCl_2$	H_2O	130	–	165	14.3%	Packed column	–	–	216	[123]
$CaCl_2$	NH_3	99	30	62	0	Packed bed	0.61	1043	200.7	[40]
$MnCl_2$	NH_3	156	35	170	35–50	Packed bed	0.703	1866.32	–	[124]
$MnCl_2$	NH_3	174	20	50	20	Packed bed	0.48	1391	179	[112]
$MnCl_2$/$SrCl_2$	NH_3	137	20	45	20	Packed bed	0.18	672.49	73.68	[111]
$MnCl_2$/$SrCl_2$	NH_3	177	20	45	20	Packed bed	0.48	2385.58	261.35	[111]
$CaCl_2$/$MnCl_2$/ENG-TSA	NH_3	130	15	40	15	Packed bed	0.45	580	–	[125]
$MnCl_2$-$CaCl_2$-NH_4Cl	NH_3	155	20	60–133	20	Packed bed	–	3474	–	[126]
$SrCl_2$/ENG-TSA	NH_3	94	25	35	15	Packed bed	0.41	706	–	[51]
$SrCl_2$	NH_3	92	–5	40	–5	Packed bed	0.687	1630.78	179	[109]
$SrCl_2$	NH_3	81	35	99	35–50	Packed bed	0.519	1851.76	–	[124]
Zeolite 13X/ENG-TSA	H_2O	250	–	25–90	–	Packed column	0.38–0.49	561.2	104.9	[110]
Zeolite 13X/ENG-TSA	H_2O	250	–	25–90	–	Packed column	0.496	570.2	106.5	[99]
$MgSO_4$ (15%)/Zeolite 13X/ENG-TSA	H_2O	250	–	25–90	–	Packed column	0.38–0.48	550.8	120.3	[110]
$MgSO_4$ (15%)/ Zeolite 13X/ENG-TSA	H_2O	250	–	25–90	–	Packed column	0.496	565.2	123.4	[99]
$MgSO_4$ (16.5%)/ Activated alumina	H_2O	250	–	25–90	–	Packed column	0.43	358.9	82.6	[99]
LiOH (15%)/Zeolite 13X	H_2O	150	5%	25	95%	Packed column	–	2175.0	–	[127]
LiOH (15%)/Zeolite 13X	H_2O	150	5%	25	60%	Packed column	–	887.5	–	[127]
$SrBr_2$/ENG	H_2O	80	5	35	5	Packed bed	–	–	250–400	[128]
$SrBr_2$/ENG	H_2O	80	35	35	12	Packed bed	–	–	150–240	[128]

The prototypes listed utilize a broad spectrum of working pairs, primarily focusing on water and ammonia as adsorbates. Open systems predominantly employ water-based pairs with silica gel, zeolites, or salt-impregnated composites (e.g., $CaCl_2$/Vermiculite, $SrCl_2$/Silica gel). These systems typically utilize packed columns or packed beds, though innovative vibrating beds and multi-layer packed beds have been implemented to enhance mass transfer. Closed systems often use ammonia to reach low cooling temperatures (e.g., -5°C [109]) and higher ESD, pairing it with halide salts like $CaCl_2$, $MnCl_2$, and $SrCl_2$, often embedded in ENG-TSA to improve thermal conductivity [51].

The operational flexibility of these prototypes is demonstrated by the wide range of charging (regeneration) temperatures (t_g) and discharging conditions reported. Several systems, such as $CaCl_2$/Silica gel [105] and $SrBr_2$ [41] prototypes, operate effectively with heat sources between 60°C and 80°C, making them suitable for low-grade waste heat or solar thermal integration. In contrast, zeolite-based closed systems often require higher temperatures, with some prototypes regenerated at 250°C to fully exploit their sorption potential [99,110].

The energy storage performance is evaluated through ESE and ESD, showing distinct trends between system types. Closed systems using ammonia generally exhibit significantly higher mass-specific ESD. For instance, a $MnCl_2$-$CaCl_2$-NH_4Cl prototype achieved a remarkable mass-specific ESD of 3474 J/g [126]. In water-based systems, chemical sorption materials like $SrBr_2$ in an open-packed bed reached a mass-specific ESD of 1130.4 J/g [41].

Overall, Table 4 highlights distinct characteristics rather than a universal performance ranking between open and closed S-TCES systems. Open systems generally offer simpler configurations and are well suited to heating and dehumidification. However, because the sorbent is in direct contact with ambient air, open systems are susceptible to contamination by airborne dust and other pollutants [129], which may accumulate on the sorbent surface, block pores, and deteriorate heat and mass transfer performance. Closed systems provide greater flexibility for heating and cooling but require hermetic, pressure-compatible

containment and additional heat-exchange components. Because the reported ESD and ESE values come from different working pairs, operating conditions, and, particularly for ESE, different energy boundaries, they should not be used directly to rank open and closed systems overall.

5. Quantifying the material-to-prototype discrepancy

The comprehensive review of material characterization and system prototyping reveals a pivotal challenge in advancing S-TCES technology: translating theoretical potential into practical engineering reality. This section discusses the statistical disparity between material-level and prototype-level performance, analyzes the root causes, and outlines future research directions to bridge this gap.

A statistical analysis of the data collected in this review (shown in Tables 3 and 4 and visualized in Fig. 10) reveals a stark discrepancy between the intrinsic performance of adsorbents and the realized performance of prototypes. The scatter plot correlates the volumetric ESD with charging temperature for both individual materials (orange circles) and integrated prototypes (green triangles).

A statistical comparison of the literature data collected in Tables 3 and 4 reveals a pronounced difference between the reported material- and prototype-level volumetric ESD values. It should be emphasized that these datasets are independently compiled rather than composed of one-to-one matched material–prototype pairs. The material-level dataset contains 43 data points, with a mean ESD of 349.4 kWh/m^3, a standard deviation of 204.1 kWh/m^3, and a median of 290.0 kWh/m^3. In comparison, the 24 prototype-level data points exhibit a substantially lower mean ESD. Using the midpoint for entries reported as ranges, the prototype-level mean is 159.5 kWh/m^3 with a standard deviation of 66.8 kWh/m^3, corresponding to a dataset-level difference of 54.3%. A sensitivity analysis using the lower and upper bounds of the reported ESD ranges gives differences of 56.0% and 52.7%, respectively. Therefore, the observed difference is robust to the treatment of range-valued data, although its precise magnitude should not be interpreted as a universal scale-up penalty.

Because the two datasets differ in sorbent composition, adsorbates, operating conditions, reactor configuration, and measurement methods, the observed material-to-prototype difference reflects the combined effects of scale-dependent heat and mass transfer limitations and dataset heterogeneity. It therefore cannot be attributed exclusively to reactor scale-up. Nevertheless, subgroup analysis by charging temperature shows consistently lower prototype-level ESD: the mean differences are approximately 36.0%, 60.9%, and 60.5% for charging temperatures of $\leq$100°C, 100–150°C, and >150°C, respectively. This consistency suggests that the overall material-to-prototype performance gap remains evident even after partially accounting for differences in charging temperature.

It should be noted that charging temperature is used here as a common descriptive variable rather than a complete representation of the thermodynamic driving force. S-TCES performance is also affected by sorbate partial pressure, relative humidity, adsorption temperature, regeneration extent, and the working pair. Because these parameters are not consistently reported across the literature, a fully normalized comparison is currently not feasible. To partially reduce the influence of working-pair heterogeneity, an additional subgroup analysis was performed for H_2O-based systems. The mean volumetric ESD of the H_2O-based material dataset is 349.4 ± 204.1 kWh/m^3, whereas that of the H_2O-based prototype dataset is 154.5 ± 67.5 kWh/m^3, corresponding to a 55.8% difference. Furthermore, the mean prototype-level ESD values are 151.2 ± 62.7 kWh/m^3 for open H_2O systems and 158.2 ± 76.2 kWh/m^3 for closed H_2O systems. These results indicate that the observed cross-scale gap remains evident even after partially controlling for the working pair and system configuration.

Although ESD is used as the principal metric in the present cross-scale comparison, it should not be regarded as a complete representation of system performance. This emphasis reflects the current development stage of S-TCES, for which most studies still focus primarily on storage capacity and ESD. ESE has also been summarized for representative prototypes, but the reported values vary substantially because of differences in system configuration, operating conditions, heat-loss treatment, and metric definitions. Data on power density, kinetics, cycle duration, pressure drop, auxiliary energy demand, and long-term cycling performance are even less consistently reported, preventing a reliable quantitative cross-scale comparison. Future assessments should therefore move toward a multidimensional framework incorporating capacity, rate, efficiency, hydraulic performance, auxiliary consumption, and durability.

This discrepancy arises because material-level tests (e.g., TG, DSC)

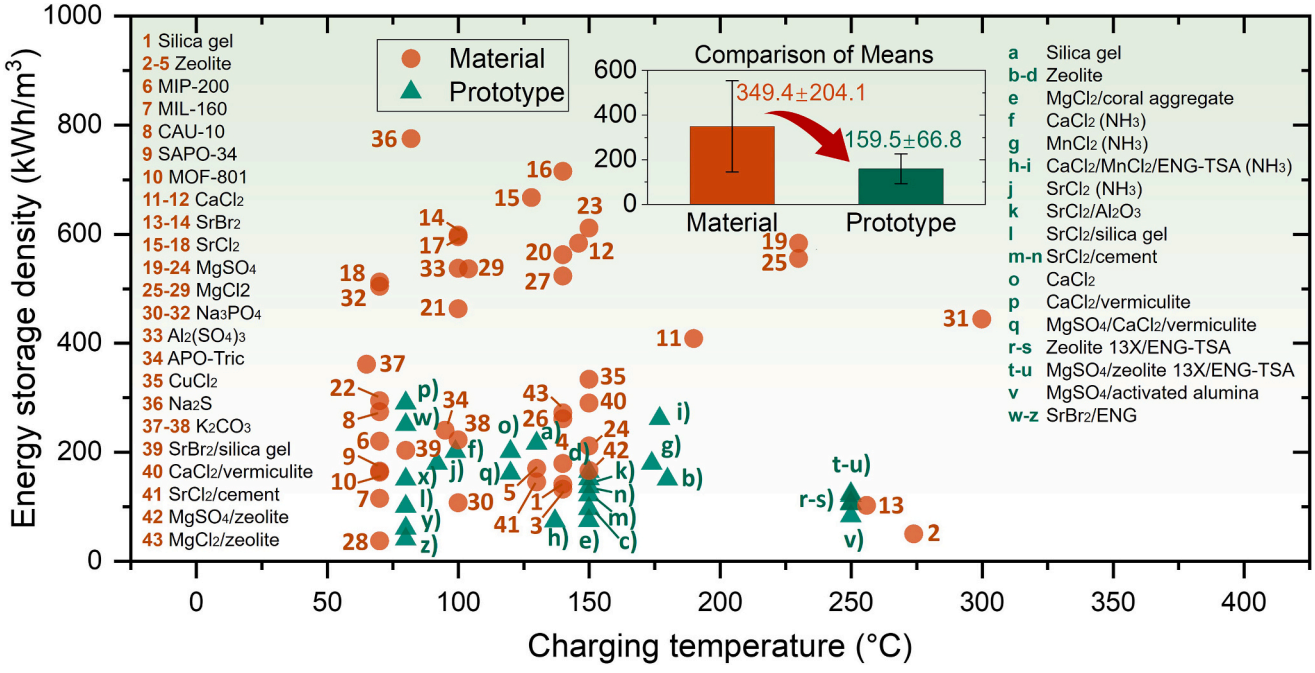


Fig. 10. Comparison of ESD derived from material-level and prototype-level tests.

measure the intrinsic capability of a few milligrams of sample under ideal, static equilibrium conditions. In contrast, prototype-level performance is penalized by engineering factors:

1) To ensure sufficient vapor permeability, packed beds require significant void space (porosity), which reduces the bulk density of the active material compared to the crystal density.
2) In large-scale reactors, heat and mass transfer resistances prevent the adsorbent from reaching the full saturation capacity observed in small-scale equilibrium tests within a practical cycle time.
3) Material characterization is typically conducted over short time scales in thermally controlled chambers that ensure a stable atmosphere with negligible heat loss. Conversely, prototype testing often spans hours or even days under realistic environmental conditions. During these prolonged periods of charging, storage, and discharging, the sensible heat dissipation to the ambient environment becomes a substantial and unavoidable energy penalty that is not captured in material-scale analysis.

To avoid confusion among scholars and industrial stakeholders, it is essential to clearly distinguish these metrics. Material-level ESD serves as the theoretical upper limit and a screening metric for material scientists. However, prototype-level ESD is the accurate indicator of commercial viability. Literature that conflates these two without qualification risks creating unrealistic expectations, potentially undermining industrial confidence in S-TCES technology. Current screening protocols typically rely on static equilibrium isotherms. However, they fail to capture dynamic behaviours crucial for S-TCES, such as the impact of heat source and heat sink temperatures and adsorption kinetics under pressure constraints. Future research should move beyond static characterization toward “lab-scale dynamic prototyping”. Instead of leaping directly to full-scale pilots, researchers should develop standardized, simplified modular testers. These setups should: (1) simulate the coupled heat and mass transfer environment; (2) incorporate realistic boundary conditions, specifically the evaporator temperature (which dictates vapor pressure) and the condenser temperature. By adopting such a “bridge” testing standard, the disparity shown in Fig. 10 can be anticipated and mitigated at the material selection stage, ensuring that only materials with robust dynamic performance proceed to system integration.

Based on the identified prototype-level bottlenecks, future material development should pivot from solely chasing high equilibrium capacity to optimizing transport properties and stability:

1) Enhancing thermal conductivity: Developing composite sorbents with highly conductive matrices (e.g., expanded graphite, carbon nanotubes) or coating technologies can enable faster, more complete reactions, improving prototype-level ESD.
2) Structural stability and cycle life: For chemical and composite adsorbents, issues like swelling, agglomeration, and deliquescence remain critical failure modes. Future work must focus on encapsulation technologies and rigid host matrices that can accommodate volume expansion without compromising bed permeability over thousands of cycles.

In conclusion, while high-performance materials are the foundation of S-TCES, the path to commercialization requires a paradigm shift. By acknowledging and addressing the engineering penalties quantified in this review, particularly the impacts of thermal mass, void fraction, and heat loss, the community can develop next-generation materials and reactor designs that effectively bridge the gap between laboratory potential and real-world application.

6. Conclusion

This review has provided a comprehensive synthesis of the state-of-the-art in sorption-based thermochemical energy storage (S-TCES) technology, from the microscopic engineering of adsorbent materials to the macroscopic optimization of prototype reactors. By systematically analyzing the thermophysical properties of physical, chemical, and composite adsorbents, and correlating them with the operational performance of open and closed systems, the following key conclusions are drawn:

1. Composite adsorbents have emerged as promising candidates for practical S-TCES applications because they can balance sorption capacity, stability, and transport properties. However, their superiority at the reactor and prototype levels has not yet been conclusively demonstrated under matched operating conditions. Moreover, synthesizing these materials remains a delicate balancing act. While salt impregnation significantly boosts energy storage density, it often introduces challenges related to pore blockage and mass transfer resistance. The review highlights that optimizing the host matrix structure to accommodate salt expansion without compromising permeability is critical for long-term cycling stability.
2. The transition from laboratory characterization to prototype operation reveals a significant performance attenuation. A cross-literature comparison reveals that the mean volumetric ESD reported for operational prototypes is approximately 52–56% lower than that reported from material-level characterization. This difference should not be interpreted as a universal scale-up penalty, because the two datasets differ in material composition, working pairs, operating conditions, and testing methodologies. Nevertheless, it highlights the substantial challenge involved in translating high intrinsic material performance into prototype-level energy storage density. This drastic reduction is primarily attributed to engineering constraints, including the necessary void fraction in packed beds, incomplete reactions, and substantial heat losses during extended operation cycles.
3. Open and closed systems have evolved along distinct trajectories to address these constraints. Open systems, while mechanically simple and cost-effective for space heating and dehumidification, are often limited by low volumetric compactness. Conversely, closed systems, particularly those utilizing ammonia-salt pairs, offer exceptional energy densities and versatile heating/cooling outputs but face higher structural complexity due to hermetic pressure containment and indirect heat-transfer requirements.

To bridge the “Valley of Death” between material science and engineering application, future research must pivot towards dynamic performance validation. Research efforts should prioritize improving thermal conductivity to enable faster, more complete reactions, reducing reliance on bulky, metal-intensive heat exchangers. The community must move beyond static equilibrium isotherms. Developing standardized, lab-scale dynamic testing protocols that account for realistic boundary conditions, such as finite heat transfer rates and coupled pressure-temperature swings, is essential for accurately predicting prototype-level behaviour. In summary, realizing the full potential of S-TCES requires a holistic approach that integrates advanced material synthesis with innovative reactor thermal design. Addressing both intrinsic transport limitations and engineering challenges will be key to making S-TCES a cornerstone technology for global carbon neutrality.

CRediT authorship contribution statement

Mingxi Ji: Writing – original draft, Visualization, Methodology, Investigation, Conceptualization. **Zhixiong Ding:** Writing – review & editing, Writing – original draft, Visualization, Software, Methodology, Investigation, Conceptualization. **Jinhan Mo:** Writing – review & editing, Visualization, Project administration, Methodology. **Yulong Ding:** Writing – review & editing, Visualization.

Declaration of competing interest

The authors declare that they have no known competing financial interests or personal relationships that could have appeared to influence the work reported in this paper.

Acknowledgments

The authors gratefully acknowledge the support from the National Natural Science Foundation of China (No. 52325801).

Data availability

Data will be made available on request.

References

[1] Ashina C, Pugazhenthiran N, Mangalaraja R, Sathishkumar P. Review on enhancing solar photocatalysis for sustainable degradation of invisible environmental pollutants. Renew Sust Energ Rev 2025;214:115490.
[2] Ding Z, Wu W. "Solution" for future heating and cooling towards carbon neutrality. Energy Rev 2026;5(1):100177.
[3] Lin H, Song Y, Ding Z, Sui Y, Sui Z, Li F, et al. Multi-stage power-to-water battery synergizes flexible energy storage and efficient atmospheric water harvesting. Nat Commun 2025;16:11098.
[4] Geng Y, Tang H, Ji W, Lin B. Mobile energy storage (MES): a grid-edge technology for power redistribution and resilience enhancement. Energy Use 2025;1(2):100022.
[5] Zhang X, Zhang R, Feng C, Wang Y, Zhao M, Zhao X. Decomposition analysis of renewable energy demand and coupling effect between renewable energy and energy demand: evidence from China. Renew Energy 2024;237:121839.
[6] Ding Z, Wu W, Leung MKH. On the rational development of advanced thermochemical thermal batteries for short-term and long-term energy storage. Renew Sust Energ Rev 2022;164:112557.
[7] IEA. Renewables 2023 – analysis. IEA; 2026. https://www.iea.org/reports/renewables-2023.
[8] Ali HM, Rehman T-u, Arıcı M, Said Z, Duraković B, Mohammed HI, et al. Advances in thermal energy storage: fundamentals and applications. Prog Energy Combust Sci 2024;100:101109.
[9] Ding Z, Wu W, Leung M. Advanced/hybrid thermal energy storage technology: material, cycle, system and perspective. Renew Sust Energ Rev 2021;145:111088.
[10] Lu X, Shi C, Li X, Liu M, Qing C, Wu Y, et al. Development of a 3 in 1 high-temperature thermal energy storage material integrating sensible, latent, and thermochemical heat. Chem Eng J 2025;522:167925.
[11] Fakri H, El Fadar A. TES materials integrated in CSP plants: research trends, challenges and 3E performance analysis. Sol Energy Mater Sol Cells 2025;293:113861.
[12] Zhang J, Guo Z, Zhu Y, Zhang H, Yan M, Liu D, et al. Preparation and characterization of novel low-cost sensible heat storage materials with steel slag. J Energy Storage 2024;76:109643.
[13] Daneshazarian R, Berardi U. Nano-enhanced thermal energy storage coupled to a hybrid renewable system for a high-rise zero emission building. Energy Convers Manag 2023;291:117301.
[14] Huang X, Li M, Li Y, Yang X, He YL. Current progress in energy utilization of building systems combining solar thermal and heat storage technologies. Renew Sust Energ Rev 2026;226:116330.
[15] Liu S, Yang R, Hou C, Ma X, Luo Z, Jiu Y, et al. Ice slurry storage: a crucial role in the consumption of renewable energy in power grid. Energy Use 2025;1(1):100015.
[16] Aftab W, Usman A, Shi J, Yuan K, Qin M, Zou R. Phase change material-integrated latent heat storage systems for sustainable energy solutions. Energy Environ Sci 2021;14:4268–91.
[17] Huang X, Hu R, Gao X, Yang X, Li M-J. Study on melting process of latent heat energy storage system by nano-enhanced phase change material under rotation condition. Appl Therm Eng 2024;247:123040.
[18] Yang S, Shao X-F, Shi H-Y, Luo J-H, Fan L-W. Bubble-injection-enabled significant reduction of supercooling and controllable triggering of crystallization of erythritol for medium-temperature thermal energy storage. Sol Energy Mater Sol Cells 2022;236:111538.
[19] Xu L, Yin J, He J, Li H, Zhu L, Ning H, et al. Completely inorganic deep eutectic solvents for efficient and recyclable liquid–liquid interface catalysis. Adv Mater 2024;36(29):2313853.
[20] Yang X, Li S, Zhao J, Huang H, Deng L. Fabrication of LiOH-metal organic framework derived hierarchical porous host carbon matrix composites for seasonal thermochemical energy storage. Nano Res 2022;15:8028–38.
[21] Kiyabu S, Girard P, Siegel DJ. Discovery of salt hydrates for thermal energy storage. J Am Chem Soc 2022;144:21617–27.
[22] Romaní J, Gasia J, Solé A, Takasu H, Kato Y, Cabeza LF. Evaluation of energy density as performance indicator for thermal energy storage at material and system levels. Appl Energy 2019;235:954–62.
[23] Ding Z, Sui Y, Zhai C, Sui Z, Lin H, Li F, et al. Transient supply-demand matching and numerical parametric study of solar absorption thermal battery for space cooling. Energy Convers Manag 2023;288:117177.
[24] Ding Z, Sui Y, Lin H, Luo X, Wang H, Chen Y, et al. Experimental study on a two-stage absorption thermal battery with absorption-enhanced generation for high storage density and extremely low charging temperature (~ 50° C). Appl Energy 2024;363:123050.
[25] Ding Z, Sui Y, Wu W. Absorption thermal battery: a rising frontier for efficient thermal utilization and renewable integration. Energy Use 2025;1(1):100002.
[26] Wu W. Low-temperature compression-assisted absorption thermal energy storage using ionic liquids. Energy Built Environ 2020;1(2):139–48.
[27] Ding Z, Sui Y, Sui Z, Lin H, Li F, Wu W. Solar-driven hygroscopic-material-based absorption thermal battery for global heating decarbonization. Energy Storage Mater 2025;77:104184.
[28] Li G, Hwang Y, Radermacher R. Review of cold storage materials for air conditioning application. Int J Refrig 2012;35:2053–77.
[29] Fan Y, Zhang W, Chen S, Zhang X, Liu X, van der Pal M, et al. A solar adsorption thermal battery for seasonal energy storage. Cell Report Phys Sci 2025;6(3):102467.
[30] Liu X, Yang F, Liu X, Wu Y. A systematic evaluation of sorption-based thermochemical energy storage for building applications: material development, reactor design, and system integration. Renew Energy 2025;245:122831.
[31] Carrasco J, Klimeš J, Michaelides A. The role of van der Waals forces in water adsorption on metals. J Chem Phys 2013;138(2):024708.
[32] Li W, Klemeš JJ, Wang Q, Zeng M. Salt hydrate–based gas-solid thermochemical energy storage: current progress, challenges, and perspectives. Renew Sust Energ Rev 2022;154:111846.
[33] Marie LF, Landini S, Bae D, Francia V, O'Donovan TS. Advances in thermochemical energy storage and fluidised beds for domestic heat. J Energy Storage 2022;53:105242.
[34] Marín PE, Milian Y, Ushak S, Cabeza LF, Grágeda M, GSF Shire. Lithium compounds for thermochemical energy storage: a state-of-the-art review and future trends. Renew Sust Energ Rev 2021;149:111381.
[35] Yan T, Li T, Xu J, Chao J, Wang R, Aristov YI, et al. Ultrahigh-energy-density sorption thermal battery enabled by graphene aerogel-based composite sorbents for thermal energy harvesting from air. ACS Energy Lett 2021;6:1795–802.
[36] Wu SF, Wang LW, An GL, Zhang B. Excellent ammonia sorption enabled by metal-organic framework nanocomposites for seasonal thermal battery. Energy Storage Mater 2023;54:822–35.
[37] Mazur N, Blijlevens MAR, Ruliaman R, Fischer H, Donkers P, Meekes H, et al. Revisiting salt hydrate selection for domestic heat storage applications. Renew Energy 2023;218:119331.
[38] Kant K, Pitchumani R. Advances and opportunities in thermochemical heat storage systems for buildings applications. Appl Energy 2022;321:119299.
[39] Hua W, Yan H, Zhang X, Xu X, Zhang L, Shi Y. Review of salt hydrates-based thermochemical adsorption thermal storage technologies. J Energy Storage 2022;56:106158.
[40] Li T, Wang R, Kiplagat JK, Kang Y. Performance analysis of an integrated energy storage and energy upgrade thermochemical solid–gas sorption system for seasonal storage of solar thermal energy. Energy 2013;50:454–67.
[41] Michel B, Mazet N, Neveu P. Experimental investigation of an innovative thermochemical process operating with a hydrate salt and moist air for thermal storage of solar energy: global performance. Appl Energy 2014;129:177–86.
[42] Farcot L, Le Pierrès N, Fourmigué J-F. Experimental investigation of a moving-bed heat storage thermochemical reactor with SrBr2/H2O couple. J Energy Storage 2019;26:101009.
[43] Stengler J, Linder M. Thermal energy storage combined with a temperature boost: an underestimated feature of thermochemical systems. Appl Energy 2020;262:114530.
[44] Wu S-F, Wang L-W, An G-L, Zhang B. Excellent ammonia sorption enabled by metal-organic framework nanocomposites for seasonal thermal battery. Energy Storage Mater 2023;54:822–35.
[45] Zhang Y, Fan Y, Zhang W, Thinsurat K, Zhang X, Jiang L. A compression-assisted sorption heat transformer for industrial heating application: working pairs and thermodynamics. Energy 2025;327:136418.
[46] Wang L, Ji M, Luo Y, Wang Y, Hu J. Research progress on solid adsorption materials for low-temperature thermal storage in buildings. J Energy Storage 2025;138:118571.
[47] Yang H, Wang C, Tong L, Yin S, Wang L, Ding Y. Salt hydrate adsorption material-based thermochemical energy storage for space heating application: a review. Energies 2023;16(6):2875.
[48] Li W, Guo H, Zeng M, Wang Q. Performance of SrBr2·6H2O based seasonal thermochemical heat storage in a novel multilayered sieve reactor. Energy Convers Manag 2019;198:111843.
[49] Aydin D, Casey SP, Chen X, Riffat S. Numerical and experimental analysis of a novel heat pump driven sorption storage heater. Appl Energy 2018;211:954–74.
[50] Kant K, Shukla A, Smeulders DMJ, Rindt CCM. Analysis and optimization of the closed-adsorption heat storage bed performance. J Energy Storage 2020;32:101896.
[51] Li TX, Wu S, Yan T, Wang RZ, Zhu J. Experimental investigation on a dual-mode thermochemical sorption energy storage system. Energy 2017;140:383–94.
[52] Zhang Y, Zhang L, Qiu J, Wang H, Zheng X, Zhang X, et al. Compressor-assisted sorption heat transformer for stable heat output in industrial application. Energy Convers Manag 2025;343:120202.

[53] Jiang L, Ji Y, Shi W, Fan Y, Wang R, Zhang X, et al. Compression-assisted adsorption thermal battery based on composite sorbent for heat supply in alpine cold region. J Energy Storage 2023;63:107033.
[54] Zbair M, Bennici S. Survey summary on salts hydrates and composites used in thermochemical sorption heat storage: a review. Energies 2021;14(11):3105.
[55] Wu H, Salles F, Zajac J. A critical review of solid materials for low-temperature thermochemical storage of solar energy based on solid-vapour adsorption in view of space heating uses. Molecules 2019;24:945.
[56] Fumey B, Weber R, Baldini L. Sorption based long-term thermal energy storage–process classification and analysis of performance limitations: a review. Renew Sust Energ Rev 2019;111:57–74.
[57] ElBahloul AA, Zeidan E-SB, El-Sharkawy II, Hamed AM, Radwan A. Recent advances in multistage sorption thermal energy storage systems. J Energy Storage 2022;45:103683.
[58] Lefebvre D, Tezel FH. A review of energy storage technologies with a focus on adsorption thermal energy storage processes for heating applications. Renew Sust Energ Rev 2017;67:116–25.
[59] Zhang Y, Wang R. Sorption thermal energy storage: concept, process, applications and perspectives. Energy Storage Mater 2020;27:352–69.
[60] Zhang W, Mehari A, Zhang X, Roskilly A, Jiang L. Ammonia-based sorption thermal battery: concepts, thermal cycles, applications, and perspectives. Energy Storage Mater 2023;62:102930.
[61] Zeng Z, Zhao B, Wang R. Water based adsorption thermal battery: sorption mechanisms and applications. Energy Storage Mater 2023;54:794–821.
[62] Zhang R, Du Y, Li X, Zhu T, Lei B, Wu Y. Sorption thermal energy storage: advances and prospects from key materials towards system integration. Appl Therm Eng 2026;302:132026.
[63] Scapino L, Zondag HA, Van Bael J, Diriken J, Rindt CCM. Sorption heat storage for long-term low-temperature applications: a review on the advancements at material and prototype scale. Appl Energy 2017;190:920–48.
[64] N'Tsoukpoe KE, Liu H, Le Pierrès N, Luo L. A review on long-term sorption solar energy storage. Renew Sust Energ Rev 2009;13:2385–96.
[65] Krese G, Koželj R, Butala V, Stritih U. Thermochemical seasonal solar energy storage for heating and cooling of buildings. Energ Buildings 2018;164:239–53.
[66] Yu N, Wang RZ, Wang LW. Sorption thermal storage for solar energy. Prog Energy Combust Sci 2013;39:489–514.
[67] Wu W, Bai Y, Huang H, Ding Z, Deng L. Charging and discharging characteristics of absorption thermal energy storage using ionic-liquid-based working fluids. Energy 2019;189:116126.
[68] Zhang X, Xun H, Zhou Y, Zhang Q, Li R, Wu X, et al. Research progress on thermochemical adsorption heat storage technology of porous matrix loaded hydrated salt. J Energy Storage 2025;128:117040.
[69] N'Tsoukpoe KE, Schmidt T, Rammelberg HU, Watts BA, Ruck WKL. A systematic multi-step screening of numerous salt hydrates for low temperature thermochemical energy storage. Appl Energy 2014;124:1–16.
[70] Yan T, Zhang H. A critical review of salt hydrates as thermochemical sorption heat storage materials: thermophysical properties and reaction kinetics. Sol Energy 2022;242:157–83.
[71] Lin J, Zhao Q, Huang H, Mao H, Liu Y, Xiao Y. Applications of low-temperature thermochemical energy storage systems for salt hydrates based on material classification: a review. Sol Energy 2021;214:149–78.
[72] Solé A, Martorell I, Cabeza LF. State of the art on gas–solid thermochemical energy storage systems and reactors for building applications. Renew Sust Energ Rev 2015;47:386–98.
[73] Palacios A, Navarro ME, Barreneche C, Ding Y. Experimental validation of thermochemical water-sorption materials for thermal energy storage: building application. Sustain Mater Technol 2023;38:e00702.
[74] Xu JX, Li TX, Chao JW, Yan TS, Wang RZ. High energy-density multi-form thermochemical energy storage based on multi-step sorption processes. Energy 2019;185:1131–42.
[75] Zhang YN, Wang RZ, Zhao YJ, Li TX, Riffat SB, Wajid NM. Development and thermochemical characterizations of vermiculite/SrBr2 composite sorbents for low-temperature heat storage. Energy 2016;115:120–8.
[76] Wang Q, Xie Y, Ding B, Yu G, Ye F, Xu C. Structure and hydration state characterizations of MgSO4-zeolite 13x composite materials for long-term thermochemical heat storage. Sol Energy Mater Sol Cells 2019;200:110047.
[77] Chen Z, Zhang Y, Zhang Y, Su Y, Riffat S. A study on vermiculite-based salt mixture composite materials for low-grade thermochemical adsorption heat storage. Energy 2023;278:127986.
[78] Yu N, Wang RZ, Lu ZS, Wang LW. Development and characterization of silica gel–LiCl composite sorbents for thermal energy storage. Chem Eng Sci 2014;111:73–84.
[79] Bales C, Gantenbein P, Hauer A, Henning H-M, Jaenig D, Kerskes H, et al. Thermal properties of materials for thermo-chemical storage of solar heat. A report of iea solar heating and cooling programme–task 32. Report B2 of Subtask B. 2005.
[80] Rezk A, Olabi AG, Alami AH, Radwan A, Demir H, Rahman SMA, et al. Experimental study on utilizing silica gel with ethanol and water for adsorption heat storage. Energies 2022;16:444.
[81] Kerskes H. Thermochemical energy storage. Storing Energy 2016:345–72.
[82] Ait Ousaleh H, Said S, Zaki A, Faik A, El Bouari A. Silica gel/inorganic salts composites for thermochemical heat storage: improvement of energy storage density and assessment of cycling stability. Mater Today Proc 2020;30:937–41.
[83] Barreneche C, Fernández AI, Cabeza LF, Cuypers R. Thermophysical characterization and thermal cycling stability of two TCM: CaCl 2 and zeolite. Appl Energy 2015;137:726–30.
[84] Clark R-J, Farid M. Experimental investigation into cascade thermochemical energy storage system using SrCl2-cement and zeolite-13X materials. Appl Energy 2022;316:119145.
[85] Wang S, Lee JS, Wahiduzzaman M, Park J, Muschi M, Martineau-Corcos C, et al. A robust large-pore zirconium carboxylate metal–organic framework for energy-efficient water-sorption-driven refrigeration. Nat Energy 2018;3:985–93.
[86] Mehrabadi A, Farid M. New salt hydrate composite for low-grade thermal energy storage. Energy 2018;164:194–203.
[87] Zhao YJ, Wang RZ, Zhang YN, Yu N. Development of SrBr2 composite sorbents for a sorption thermal energy storage system to store low-temperature heat. Energy 2016;115:129–39.
[88] Clark R-J, Gholamibozanjani G, Woods J, Kaur S, Odukomaiya A, Al-Hallaj S, et al. Experimental screening of salt hydrates for thermochemical energy storage for building heating application. J Energy Storage 2022;51:104415.
[89] Van Essen VM, Zondag HA, Gores JC, Bleijendaal LPJ, Bakker M, Schuitema R, et al. Characterization of MgSO4 hydrate for thermochemical seasonal heat storage. J Solar Energy Eng 2009;131(4):041014.
[90] Sögütoglu LC, Donkers PAJ, Fischer HR, Huinink HP, Adan OCG. In-depth investigation of thermochemical performance in a heat battery: cyclic analysis of K2CO3, MgCl2 and Na2S. Appl Energy 2018;215:159–73.
[91] Ristić A, Logar NZ, Henninger SK, Kaučič V. The performance of small-pore microporous aluminophosphates in low-temperature solar energy storage: the structure–property relationship. Adv Funct Mater 2012;22:1952–7.
[92] Donkers PAJ, Pel L, Adan OCG. Experimental studies for the cyclability of salt hydrates for thermochemical heat storage. J Energy Storage 2016;5:25–32.
[93] Fotia A, Brancato V, Mastronardo E, Calabrese L, Frazzica A. Enhancement of CaCl2/silica gel composites sorbent stability for low-grade thermal energy storage. J Energy Storage 2025;132:117679.
[94] Frazzica A, Brancato V, Caprì A, Cannilla C, Gordeeva LG, Aristov YI. Development of "salt in porous matrix" composites based on LiCl for sorption thermal energy storage. Energy 2020;208:118338.
[95] Brancato V, Gordeeva LG, Sapienza A, Palomba V, Vasta S, Grekova AD, et al. Experimental characterization of the LiCl/vermiculite composite for sorption heat storage applications. Int J Refrig 2019;105:92–100.
[96] Courbon E, D'Ans P, Permyakova A, Skrylnyk O, Steunou N, Degrez M, et al. A new composite sorbent based on SrBr2 and silica gel for solar energy storage application with high energy storage density and stability. Appl Energy 2017;190:1184–94.
[97] Casey SP, Aydin D, Elvins J, Riffat S. Salt impregnated desiccant matrices for 'open' thermochemical energy conversion and storage – improving energy density utilisation through hygrodynamic & thermodynamic reactor design. Energy Convers Manag 2017;142:426–40.
[98] Hongois S, Kuznik F, Stevens P, Roux J-J. Development and characterisation of a new MgSO4−zeolite composite for long-term thermal energy storage. Sol Energy Mater Sol Cells 2011;95:1831–7.
[99] Xu SZ, Wang RZ, Wang LW, Zhu J. Performance characterizations and thermodynamic analysis of magnesium sulfate-impregnated zeolite 13X and activated alumina composite sorbents for thermal energy storage. Energy 2019;167:889–901.
[100] Erlund R, Zevenhoven R. Thermal energy storage (TES) capacity of a lab scale magnesium hydro carbonates/silica gel system. J Energy Storage 2019;25:100907.
[101] Kim H, Hong SK, Kang JG, Moon S-W, Kim G-h, Yoon S, et al. Exploration adsorption characteristics of zeolite 13X depending on humidity and flow rate in sorption thermal energy storage applications. Int J Heat Mass Transf 2024;221:125049.
[102] Qiu Y, Yang Y, Yang N, Tong L, Yin S, Wang L, et al. Thermochemical energy storage using silica gel: thermal storage performance and nonisothermal kinetic analysis. Sol Energy Mater Sol Cells 2023;251:112153.
[103] Zhang Y, Wang R, Li T. Experimental investigation on an open sorption thermal storage system for space heating. Energy 2017;141:2421–33.
[104] Aydin D, Casey SP, Chen X, Riffat S. Novel "open-sorption pipe" reactor for solar thermal energy storage. Energy Convers Manag 2016;121:321–34.
[105] Wyttenbach J, Bougard J, Descy G, Skrylnyk O, Courbon E, Frère M, et al. Performances and modelling of a circular moving bed thermochemical reactor for seasonal storage. Appl Energy 2018;230:803–15.
[106] Zhang Y, Yan T, Wang R. A new strategy of dual-material reactors for stable thermal output of sorption thermal battery. Energy 2024;293:130692.
[107] Zhu J, Gao C, Kong F, Zhang K, Bai Z, Guo J. Low-priced stable SrCl2@ SG composite sorbents for low-grade solar heat storage application in open sorption systems. Sol Energy Mater Sol Cells 2021;229:111118.
[108] Zhao YJ, Wang RZ, Li TX, Nomura Y. Investigation of a 10 kWh sorption heat storage device for effective utilization of low-grade thermal energy. Energy 2016;113:739–47.
[109] Zhang H, Yan T, Yu N, Wang C. Experimental investigation on a strontium chloride/ammonia sorption heat storage system. Appl Therm Eng 2023;219:119478.
[110] Xu SZ, Wang RZ, Wang LW, Zhu J. A zeolite 13X/magnesium sulfate–water sorption thermal energy storage device for domestic heating. Energy Convers Manag 2018;171:98–109.
[111] Yan T, Kuai Z, Wu S. Experimental investigation on a MnCl2–SrCl2/NH3 thermochemical resorption heat storage system. Renew Energy 2020;147:874–83.
[112] Yan T, Wang RZ, Li TX. Experimental investigation on thermochemical heat storage using manganese chloride/ammonia. Energy 2018;143:562–74.

[113] Tso C, Chan K, Chao CY, Wu C. Experimental performance analysis on an adsorption cooling system using zeolite 13X/CaCl2 adsorbent with various operation sequences. Int J Heat Mass Transf 2015;85:343–55.
[114] Abohamzeh E, Hosseinizadeh SE, Frey G. Numerical investigation and response surface optimization of a sorption heat storage systems performance using Y-shaped fins. J Energy Storage 2024;84:110803.
[115] Strong C, Carrier Y, Tezel FH. Experimental optimization of operating conditions for an open bulk-scale silica gel/water vapour adsorption energy storage system. Appl Energy 2022;312:118533.
[116] Wang L, Luo Y, Guo S, Yang G. Experimental investigation on the thermochemical energy storage performance of MgCl2-coral aggregate composites. J Energy Storage 2025;116:116075.
[117] Clark R-J, Farid M. Experimental investigation into the performance of novel SrCl2-based composite material for thermochemical energy storage. J Energy Storage 2021;36:102390.
[118] Yang G, Ji M, Huang Y, She X, Luo Y, Wang L, et al. Characterization and performance analysis of SrCl2 impregnated activated alumina composites for solar thermal energy storage. Sol Energy Mater Sol Cells 2025;282:113385.
[119] Yang H, Wang C, Zhang Y, Nie B, Tong L, Yin S, et al. Experimental investigation of a thermochemical energy storage system based on MgSO4-silica gel for building heating: adsorption/desorption performance testing and system optimization. Energy Convers Manag 2024;301:118000.
[120] Zondag H, Kikkert B, Smeding S, Boer Rd, Bakker M. Prototype thermochemical heat storage with open reactor system. Appl Energy 2013;109:360–5.
[121] Köll R, van Helden W, Engel G, Wagner W, Dang B, Jänchen J, et al. An experimental investigation of a realistic-scale seasonal solar adsorption storage system for buildings. Sol Energy 2017;155:388–97.
[122] Yu N, Wang RZ, Wang LW. Theoretical and experimental investigation of a closed sorption thermal storage prototype using LiCl/water. Energy 2015;93:1523–34.
[123] Richter M, Bouché M, Linder M. Heat transformation based on CaCl2/H2O – part a: closed operation principle. Appl Therm Eng 2016;102:615–21.
[124] Yan T, Wang CY, Li D. Performance analysis of a solid-gas thermochemical composite sorption system for thermal energy storage and energy upgrade. Appl Therm Eng 2019;150:512–21.
[125] Jiang L, Wang R, Wang L, Roskilly A. Investigation on an innovative resorption system for seasonal thermal energy storage. Energy Convers Manag 2017;149:129–39.
[126] ElBahloul AA, Zeidan E-SB, El-Sharkawy II, Hamed AM, Radwan A. Experimental and numerical investigation of multistage sorption energy storage system. Appl Therm Eng 2023;218:119313.
[127] Jung DY, Choi HW, Jeong J, Kim Y, Kim J, Choi J, et al. Optimization of sorption thermal battery via breakthrough curve modeling and experimental validation. Energy Convers Manag 2025;343:120252.
[128] Lahmidi H, Mauran S, Goetz V. Definition, test and simulation of a thermochemical storage process adapted to solar thermal systems. Sol Energy 2006;80:883–93.
[129] Tian E, Chen Q, Gao Y, Chen Z, Wang Y, Mo J. Advancing indoor air purification by mass transfer enhancement: bridging the gap between high-performance materials and technologies. Engineering 2026;60:246–59.